Materials Today Bio 32 (2025) 101705

Contents lists available at ScienceDirect

Materials Today Bio

journal homepage: www.journals.elsevier.com/materials-today-bio

# A cerium nanocluster for effective alleviation of inflammatory bowel disease by scavenging RONS and regulating gut microbiome

Dan Yang [a,b,1], Rong Wang [b,1], Lei Zhao [a,1], Ye Xu [c], Yufeng Zhu [b], Jingyan Zhang [d], Zhiguo Zhou [b], Yun Sun [e,*], Shiping Yang [b], Hong Yang [b,**], Wu Wang [a,***]

[a] Department of Radiology, Longhua Hospital, Shanghai University of Traditional Chinese Medicine, Shanghai, 200032, China
[b] Joint International Research Laboratory of Resource Chemistry of Ministry of Education, Shanghai Key Laboratory of Rare Earth Functional Materials, and Shanghai Frontiers Science Center of Biomimetic Catalysis, Shanghai Normal University, Shanghai, 200234, China
[c] Institute of Molecular Medicine (IMM), Renji Hospital, School of Medicine, Shanghai Jiao Tong University, Shanghai, 200240, China
[d] Institute of Metabolism and Integrative Biology, Fudan University, Shanghai, 200032, China
[e] Department of Research and Development, Shanghai Proton and Heavy Ion Center, Fudan University Cancer Hospital, Shanghai, 201321, China

ARTICLE INFO

*Keywords:*
Cerium nanocluster
Inflammatory bowel disease
RNA sequence analysis
Gut microbiome

ABSTRACT

Inflammatory bowel disease (IBD) is characterized by excessive generation of reactive oxygen species and reactive nitrogen species (RONS) within the pro-inflammatory microenvironment. Conventional treatments often have serious side effects, making IBD management challenging. Here, a new cerium cluster, Ce12, with a formula of $[Ce_{12}(\mu_3\text{-}O)_8(\mu_3\text{-}OH)_8(\mu_2\text{-}OH)_6(ADA)_{18}]\bullet 3H_2O\bullet 3CH_3CN$ ($ADA^-$ = 1-adamantanecarboxylate) was prepared and capped with β-cyclodextrin (β-CD) through self-assembly process involving the adamantane moiety of Ce12 and β-CD, resulting in Ce12@CD nanoparticles (NPs). Ce12@CD NPs, with good stability and biocompatibility, exhibit excellent reactive RONS scavenging activities due to the presence of a fraction of $Ce^{3+}$ ions, offering potential for treating inflammatory diseases. Treatment significantly alleviated body weight loss, colon length reduction, and pathological injury of colon in mice with dextran sodium sulfate (DSS)-elicited colitis, thereby repairing the intestinal mucosal barrier and reducing inflammation. RNA sequence analysis revealed that the therapeutic effects of Ce12@CD NPs are highly correlated with IL-17 and TNF signaling pathways, thereby reducing inflammatory factors such as IL-1β and TNF-α, and alleviating intestinal inflammation. Additionally, Ce12@CD NPs successfully modulated DSS-induced gut microbiota imbalances. This work highlights the unique catalytic activity of Ce12@CD NPs in removing RONS and mimicking biological enzymes, showcasing their potential therapeutic applications for inflammatory disorders.

## 1. Introduction

Inflammatory bowel disease (IBD) is a chronic, recurrent, complex and diverse gastrointestinal disease, which has become increasingly prevalent worldwide in the past decade [1]. IBD exhibits similar clinical symptoms involving abdominal discomfort, diarrhea and bloody stools [2]. In general, the intestinal mucosa of IBD is characterized by extensive infiltration of inflammatory cells [3], which triggers excessive immune activity and an elevation of pro-inflammatory cytokines, in turn, ultimately leads to a chronic, uncontrolled immune response [4–6], while regulatory immune cells and mediators are unable to maintain tissue homeostasis. Chronic active inflammation is directly related to the production and emission of reactive oxygen species (ROS), which are important signaling molecules that promote their immune function [7–9]. Despite their beneficial role in normal immune responses, the continuous release of ROS can lead to collateral damage, including malnutrition, increased intestinal permeability, and interference with intestinal motivity [10], which should be responsible for abnormal and overactive intestinal inflammation in IBD.

Current treatment of IBD aims to alleviate and mitigate complications of the disease rather than reversing the complicated underlying pathogenic mechanisms [11]. Depending upon the degree of symptom

* Corresponding author.
** Corresponding author.
*** Corresponding author.
*E-mail addresses:* yun.sun@sphic.org.cn (Y. Sun), yanghong@shnu.edu.cn (H. Yang), lh20038@shutcm.edu.cn (W. Wang).
[1] Dan Yang and Rong Wang and Lei Zhao contributed equally to this work.

https://doi.org/10.1016/j.mtbio.2025.101705
Received 27 January 2025; Received in revised form 8 March 2025; Accepted 23 March 2025
Available online 25 March 2025

severity, medications like immunomodulators, corticosteroids, aminosalicylate, etc., are used to treat IBD patients [12–15]. However, these molecules have poor stability, low bioavailability, insufficient antioxidant activity [16], and long-term use of the aforementioned conventional drugs can lead to severe adverse effects, such as pancreatitis, allergic reactions, nausea, and increased liver enzyme levels [17,18]. It is clear that the excessive reactive oxygen and nitrogen species (RONS) in the inflamed areas of the colon has become one of the potential therapeutic targets [12,19]. Currently, a number of nanomaterials have been developed that can neutralize excess RONS and alleviate inflammatory diseases, resulting in significant advances in the field of antioxidant therapy. For the treatment of colitis, the strategies of nanomaterials are primarily divided into anti-oxidation, anti-inflammatory, and modulation of gut microbiota dysbiosis. Antioxidant nanomaterial strategies include natural enzymes, nanozymes, antioxidant compounds, and natural substances. Anti-inflammatory nanomedicines involve drug-loaded nanoparticles, natural substances, and metallic/non-metallic nanomaterials. [20]. Wang et al. [21] reported for the first time an intrinsic strain-mediated ultrathin ceria nanoantioxidant. it increases the superoxide dismutase (SOD)-mimetic activity by ~2.6-fold (1533 U/mg, close to natural SOD) and total antioxidant activity by ~2.5-fold. The 2D polylysine-modified polydopamine nanosheets (PDA@PLL NSs) [22], through the integration of dimension and surface charge engineering, scavenge multiple danger signals including RONS and cfDNA, could concurrently activate the Keap1-Nrf2 pathway and block TLR9 signaling pathway, thus achieving synergistic inflammation inhibition. These commonly utilize vary-valence to clear RONS or drug-carrying nanomaterials to treat colitis, but many exhibit large and heterogeneous nanosizes, require high frequency administration by oral administration, and can lead to off-target systemic side effects [23,24] due to the challenge of targeting from the intestinal environment to the inflamed colon region [14,25]. To overcome this, nanomaterials with intrinsic enzyme-like activity have become a hotpot and have been developed recently.

Clusters have nanoscale dimensions, well-defined structures, and precise compositions, which facilitate batch repeat synthesis. Nanoceria possesses the remarkable ability to switch between two oxidation states: $Ce^{3+}$ and $Ce^{4+}$, and thus may combat oxidation and inflammation signals through its CAT and SOD-like activities [26]. Cerium oxide is considered one of the most effective and promising candidates for mimicking antioxidant enzymes. Therefore, we focused on cerium cluster with good biosafety and two stable valence states [27] and reported a novel 12-core cerium nanocluster (Ce12@CD NPs). The $Ce^{3+}/Ce^{4+}$ transformation in Ce12@CD NPs is used to simulate SOD and CAT enzyme activities, thereby clearing RONS ($H_2O_2$, ·OH, $O_2^{\cdot-}$, DPPH, ABTS) and relieving oxidative stress, thereby protecting cells from RONS induced damage. Ce12@CD NPs exhibit a faster onset of action compared to immunomodulators, without the risks of immunosuppression or infection susceptibility. Their preparation is simple, cost-effective, and they possess a favorable safety profile. In contrast to aminosalicylic acid drugs, which have limited efficacy, Ce12@CD NPs show superior therapeutic outcomes. Importantly, Ce12@CD NPs significantly mitigates colon damage in DSS induced acute colitis by alleviating inflammatory cell infiltration and modulating the reduction of pro-inflammatory cytokines, rehabilitating the intestinal barrier and ultimately regulating intestinal flora, which has excellent effects in the treatment of IBD (Scheme 1). Ce12@CD NPs has good biocompatibility and is promising to combat RONS related inflammation.

## 2. Materials and methods

### 2.1. Materials

$Ce(NH_4)_2(NO_3)_6$, $C_2H_5NO_2$, $C_{11}H_{16}O_2$, $C_{42}H_{70}O_{35}$, $C_2H_6OS$ and 4′6-diamidino-2-phenylindole (DAPI) were purchased from Adamas. Lipopolysaccharide (LPS) was purchase from Macklin. Superoxide Dismutase (SOD) Activity Detection Kit were purchased from ACMEC (Shanghai, China). Mouse IL-1β ELISA Kit, Mouse IL-6 ELISA Kit and Mouse TNF-α ELISA Kit were purchased from Multi Sciences (Lianke) Biotech Co., Ltd. Myeloperoxidase (MPO) Test Kit was from Nanjing Jiancheng Technology Co., Ltd (Nanjing, China). Total Antioxidant Capacity Assay Kit with ABTS method was purchase from Beyotime Biotechnology (Shanghai, China).

### 2.2. Characterizations

Absorption spectra, the infrared spectrum, X-ray powder diffractometer and X-ray photoelectron spectroscopy were performed on

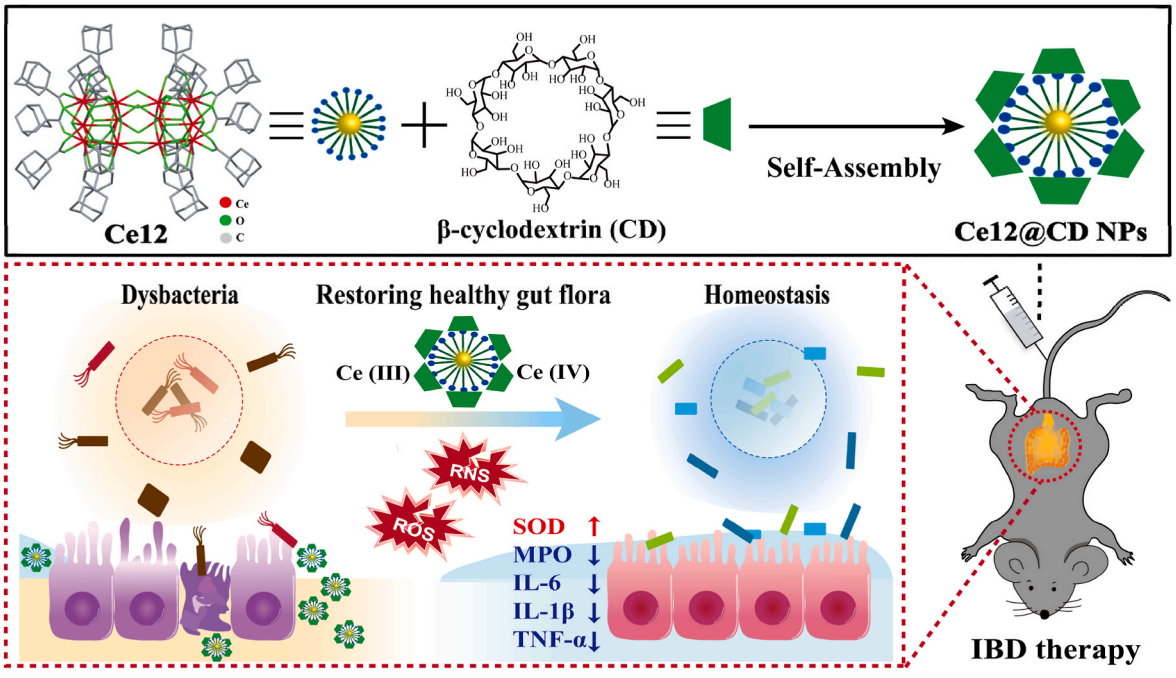


**Scheme 1.** Schematic illustration of Ce12@CD NPs with RONS scavenging for antioxidant, anti-inflammation and microbiota modulation.

Beckman Coulter DU 730 spectrometer, Nicolet A370 FT-IR spectrometer, Rigaku D/MAX 2000 diffractometer with Cu κα radiation and Perkin-Elmer PHI-5400 respectively. The hydrodynamic diameter was measured on Malvern Zetasizer Nano-ZS90. SEM images were performed on a scanning electron microscope (Hitachi S-4800). The concentration of Ce was determined by ICP-MS (VISTAMPXICP VARIAN)

### 2.3. Material synthesis

#### 2.3.1. Synthesis of Ce6 ($Ce_6$ ($\mu_3$-O)$_8$ ($\mu_6$-OH)$_4$ ($\mu_2$-$NH_2CH_2COO$)$_{10}$) precursor

Cerium ammonium nitrate (1.5 g, 2.7 mmol) dissolved in water (0.9 mL, 50 mmol), glycine (0.3 g, 4 mmol) was added and stirred for 30 min. Then the solution was diluted with saturated NaCl solution, sealed and allowed to stand for 2 days, yielding yellow-orange crystals. Filtered, washed with water and were oven-dried at 60 °C overnight to obtained the precursor Ce6.

#### 2.3.2. Synthesis of Ce12 ($Ce_{12}(\mu_3\text{-}O)_8(\mu_3\text{-}OH)_8(\mu_2\text{-}OH)_6(ADA)_{18}]\bullet 3H_2O\bullet 3CH_3CN$) clusters

0.1 g of Ce6 precursor was completely dissolved in 2 mL deionized water, and then added dropwise to DMF containing 1-adamantanecarboxylic acid (1 g, 10 mL) under sonication. The reaction mixture was magnetically stirred for 12 h at 85 °C. After the reaction, precipitate was filtrated, washed with methanol 3 times, and dried overnight.

#### 2.3.3. Synthesis of Ce12@CD NPs

Ce12 (6.3 mg, 0.5 μM) was dissolved in 16 mL DMSO, and then 2 mL β-CD (10.12 mg, 8 μM) in DMSO was dropped slowly into Ce12 during vigorous stirring. Then the mixture was stirred for another 48 h to reacted sufficiently to obtain Ce12@CD NPs. Finally, the obtained Ce12@CD NPs were dialyzed (MWCO = 8000 Da) for 48 h to remove the free reagents and DMSO. Subsequently, a stability study of Ce12@CD NPs was conducted, which included measurements of their zeta potential in water over 7 days, as well as changes in particle size over 7 days in various media: water, PBS, phosphate buffer solutions with different pH values (pH = 5.2, 6.5, and 7.4), and DMEM with 10 % serum.

### 2.4. Scavenging ROS and RNS

#### 2.4.1. OH scavenging activity of Ce12@CD NPs

3,3′,5,5’ - tetramethylbenzidine (TMB) was used as the indicator to detect the presence of hydroxyl radical (·OH) generated by Fenton reaction between hydrogen peroxide ($H_2O_2$) and ferrous ion. TMB can be oxidized and exhibit a characteristic absorption at 652 nm. Specifically, the experimental solutions were prepared under dark conditions, comprising 1 mL of $FeSO_4$ (1 mM), 1 mL of $H_2O_2$ (2 mM), 1 mL of TMB solution (1 mM), and varying concentrations of Ce12@CD NPs ranging from 50 to 250 μg mL$^{-1}$, all dissolved in an HAc/NaAc buffer solution maintained at pH 4.5. These solutions were then incubated for 5 min to allow for the reaction to proceed. Subsequently, the absorbance of the solution at 652 nm was measured by UV–VIS spectroscopy.

#### 2.4.2. $H_2O_2$ scavenging activity of Ce12@CD NPs

The $H_2O_2$ scavenging capacity of Ce12@CD NPs was evaluated by the Hydrogen Peroxide Detection Kit (Nanjing Jiancheng Bioengineering Institute, Nanjing, China). $H_2O_2$ reacts with ammonium molybdate and displays an absorbance peak at 405 nm. To evaluate the NPs’ efficacy, various concentrations of Ce12@CD NPs (50, 100, 150, 200 and 250 μg mL$^{-1}$) were individually incubated with $H_2O_2$ (2 mM) at 37 °C for 5 min, respectively. After the reaction, the UV absorbance of each solution at 405 nm was measured, and the $H_2O_2$-eliminating capacity was calculated. Each concentration was tested in three parallel groups.

#### 2.4.3. $O_2^{-\cdot}$ scavenging activity of Ce12@CD NPs

The superoxide anion ($O_2^{-\cdot}$) scavenging ability of Ce12@CD NPs was evaluated by the $O_2^{-\cdot}$ assay kit (Nanjing Jiancheng Bioengineering Institute, Nanjing, China). Different concentrations of Ce12@CD NPs (2, 4, 6, 8, and 10 μg mL$^{-1}$) were individually introduced into the working solution and mixed thoroughly. The mixtures were then incubated in a water bath at a constant temperature of 37 °C for 40 min. After the incubation, 2 mL of colorant was added, and the UV absorbance at 550 nm was subsequently determined, and the clearance rate was calculated according to the absorbance value.

#### 2.4.4. ABTS radical scavenging activity of Ce12@CD NPs

Dispense 200 μL of $ABTS^{+\cdot}$ working solution into each well of a 96-well plate. Add 10 μL of distilled water to designated wells as controls. For the test samples, add 10 μL of Ce12@CD NPs at varying concentrations (2, 4, 6, 8 and 10 μg mL$^{-1}$) to the remaining wells. Gently mix the solutions to ensure homogeneity, then incubate at room temperature for 6 min. After incubation, the absorbance at 414 nm was determined using microplate reader, and the total antioxidant capacity of the samples was calculated from the absorbance values of the different groups (n = 3).

#### 2.4.5. DPPH radical scavenging activity of Ce12@CD NPs

2,2-Diphenyl-1-picrylhydrazyl (DPPH·) is a free radical and its alcoholic solution is purple in color with strong absorption at 517 nm. Specifically, 20 μL of Ce12@CD NPs at varying concentrations (1, 5, 10, 15 and 20 μg mL$^{-1}$) or water as a control were individually added to 200 μL of the prepared 25 μM DPPH anhydrous ethanol solution, respectively. These mixtures were allowed to react at room temperature for 2 h. Then the UV–Vis absorption spectra of the solutions were measured at 517 nm to evaluate the scavenging activity of Ce12@CD NPs against DPPH radicals (n = 3).

#### 2.4.6. Catalase-like (CAT-like) activity of Ce12@CD NPs

A dissolved oxygen analyzer was used to measure $O_2$ levels in real time. 5 mL of Ce12@CD NPs (50, 100, 150 and 250 μg mL$^{-1}$) were poured into a 15 mL round-bottomed flask and seal it with sealing film, and 1 mL of 10 mM $H_2O_2$ was injected after the system reading stabilizes. The amount of dissolved $O_2$ generated was monitored every 10 s interval (n = 3).

#### 2.4.7. SOD-like activity of Ce12@CD NPs

The superoxide dismutase (SOD) activity of Ce12@CD NPs was evaluated using the SOD activity detection kit (ACMEC, Shanghai, China). Different concentrations of Ce12@CD NPs (1, 5, 10, 15 and 20 μg mL$^{-1}$) were added to the working solution, respectively, and thoroughly mixed. After a 30-min incubation at 37 °C, the absorbance of the solution at 560 nm was measured. During this process, a specific quantity of $O_2^{-\cdot}$ was generated within the system, leading to a strong absorbance at 560 nm. Ce12@CD NPs reduced $O_2^{-\cdot}$ levels, reflected by decreased UV absorbance. The clearance rate was calculated based on absorbance values (n = 3).

### 2.5. In vitro experiments

#### 2.5.1. Cell culture

RAW264.7 and HUVEC cells were cultured in DMEM medium (containing 10 % (v/v) fetal bovine serum (FBS), 1 % (v/v) penicillin and streptomycin) at 37 °C in an incubator supplied with a humidified atmosphere of 5 % $CO_2$.

#### 2.5.2. Cytotoxicity

A standard MTT assay was adopted to evaluate the cytotoxicity of Ce12@CD NPs with different concentrations (0, 10, 30, 50, 75, 100, 150, 200 μg/mL). HUVEC cells were incubated with Ce12@CD NPs with different concentrations for 12 and 24 h, respectively. After incubation,

the cell viability was determined by the standard MTT procedures. The cell viability survival rate was calculated based on the absorbance value of each well (n = 3).

#### 2.5.3. Hemolysis assay

From a healthy 6-week-old male BALB/c mouse, 1 mL of fresh blood was swiftly obtained and transferred into an EDTA-coated anti-coagulation tube. Red blood cells (RBCs) were isolated *via* centrifugation (3000 rpm, 10 min) and washed four times with PBS solution until the upper layer was clear and transparent, and finally diluted it to 10 mL with PBS. 0.2 mL diluted red blood cell suspension was mixed with 0.8 mL of deionized water (positive group, PG), PBS (negative group, NG) or PBS containing varying concentrations of Ce12@CD NPs at 10, 20, 50, 100, 150, and 200 μg/mL (experimental groups, EG), respectively. The mixtures were incubated at 37 °C for 2 h, followed by centrifuged at 3000 rpm for 5 min. After centrifugation, take photos for record and the supernatants were carefully collected for absorbance measurements at 541 nm.

The hemolysis rate is calculated using the formula below. $A_{EG}$ is the absorbance of the experimental group; $A_{NG}$ is the absorbance of negative group; $A_{PG}$ is the absorbance of the positive group.

$$\text{Hemolysis rate (\%)} = (A_{EG}\text{-}A_{NG})/\ (A_{PG}\text{-}A_{NG}) \times 100\ \%$$

#### 2.5.4. Antioxidant studies

ROS scavenging was detected with DCFH-DA probe along with the fluorescent change from fluorescent DCF to non-fluorescent DCFH.

HUVEC cells at a density of $1 \times 10^5$ were inoculated into confocal dishes and incubated for 12 h. Antioxidant capacity was assessed at the cellular level by incubating with 1 mM $H_2O_2$ to establish a nutrient stress environment in the cells.

Experimental components.

1 Control group: HUVEC without treatment
2 $H_2O_2$ group: HUVEC treated with 1 mM $H_2O_2$ treatment
3 Treatment group: HUVEC co-treated with Ce12@CD NPs (50, 100 μg/mL) and 1mM $H_2O_2$ treatment

After HUVEC were incubated with 1 mL DCFH-DA (10 μM in DMEM medium) for 20 min, then the cells of the $H_2O_2$ group were stimulated with 1 mM $H_2O_2$; the cells of treatment group were incubated with 1 mL Ce12@CD NPs (50, 100 μg/mL) and 1 mM $H_2O_2$ for 45 min. They were performed with laser confocal, selecting a 405 nm excitation source with a collection wavelength range of 440–465 nm.

#### 2.5.5. Cellular anti-inflammatory studies

ROS Indicator (DCFH-DA) was used to monitor intracellular ROS changes in macrophages (RAW264.7 cells).

① Experimental components:
② Control group: RAW264.7 without treatment
③ LPS group: RAW264.7 was treated with lipopolysaccharide (LPS, 100 ng/mL) stimulation.
④ Treatment group: Ce12@CD NPs (10, 50, 100 μg/mL) pretreated RAW264.7 for 2 h, then stimulated with LPS for 4 h.

The RAW264.7 cells were cultured in confocal dishes for 12 h. The control group: the cells in were treated with fresh medium; In other groups, the cells were stimulated with LPS (100 ng/mL); the LPS group were stimulated with LPS; subsequently, the medium was replaced with 1 mL of DCFH-DA (10 μM in DMEM medium) and incubated for 20 min. The treatment group were pretreated with the material for 2 h and then stimulated with LPS for 4 h; finally, the cells were washed with PBS for 3 times and observed with CLSM. In addition, supernatants of RAW264.7 cell cultures from each group were collected to measure the levels of pro-inflammatory factors IL-1β, IL-6 and TNF-α.

### 2.6. In vivo experiments

Animal Experiments: The animal experiments were approved and conducted in strict accordance with the requirements of the Ethics Committee of Shanghai Normal University (Shanghai, China). Male BALB/c mice were obtained from Shanghai Jiesjie Experimental Animals (Shanghai, China).

#### 2.6.1. IBD models in mice

Male BALB/c mice (6–8 weeks old, 16–20 g) were acclimatized for one week, and then the drinking water was changed to 4 % Dextran Sulfate Sodium Salt (DSS) solution for one week, and the growth condition of the mice was observed and recorded daily.

#### 2.6.2. Biosafety

BALB/c mice (n = 3) were injected intravenously with Ce12@CD NPs (10 mg/kg, 0.1 mL) on days 1, 3, 5 and 7. Major organs and blood were collected on days 9 and 16 for hematoxylin and eosin (H&E) staining and blood index analysis, including blood biochemistry and blood routine.

#### 2.6.3. In vivo distribution

Healthy BALB/c mice (n = 3) were intravenously injected with Ce12@CD NPs (10 mg/kg, 0.1 mL) to investigate the biodistribution of Ce12@CD NPs. Hearts, livers, spleens, lungs, kidneys, and colons were collected and weighed at different time points post-injection (2, 6, 12, and 24 h), followed by nitrification with aqua regia. ICP-MS was then performed to determine the content of cerium, and the biological distribution was assessed by the percentage of injected cerium per gram of tissue (%ID/g).

#### 2.6.4. Pharmacokinetics of Ce12@CD NPs

The pharmacokinetics were evaluated by intravenous injection of Ce12@CD NPs (10 mg/kg, 0.1 mL) in healthy BALB/c mice (n = 3). Blood was collected at different time points after injection (1, 2, 6, 12, and 24 h) and the urine and feces from mice were collected daily for 1 week. The concentration of Ce was measured by ICP-MS.

#### 2.6.5. Preventive effect against IBD model

For colitis prevention effect, healthy BALB/c mice were randomly assigned to four groups (n = 5 per group).

1 Control group: $H_2O$ + PBS
2 DSS group: 4 % DSS + PBS
3 Treat 1 group: 4 % DSS + Ce12@CD NPs (5 mg/kg)
4 Treat 2 group: 4 % DSS + Ce12@CD NPs (10 mg/kg)

The mice in the DSS group, treat 1 group and treat 2 group drank water containing 4 % DSS (w/v, dextran sulfate sodium) for one consecutive week (i.e., from day 0 to day 7), and then replaced by water only from day 8 to day 16. During this period, the mice in each group were injected with the corresponding material intravenously in the tail vein on days 1, 3, 5 and 7. Control group and DSS group were injected with PBS in the tail vein; Treat 1 group and treat 2 group were injected with Ce12@CD NPs (5 mg/kg) and Ce12@CD NPs (10 mg/kg) in the tail vein, respectively. Body weight data was collected daily for each group of mice and the Disease Activity Index (DAI) was assessed according to the evaluation criteria in Table 1. Over a 9-day period, body weight changes were recorded daily, and stool consistency and fecal bleeding were observed and recorded daily. In addition, in order to avoid the influence of the environment on the inflamed colon during sampling on day 9, one randomly selected colon from each group with different treatments was immediately taken for immune-histological

**Table 1**
DAI scoring criteria.

| Stoll consistency | Bleeding | Weight loss |
|---|---|---|
| Formed = 0 | Normal color = 0 | No weight loss = 0 |
| Mild soft = 1 | Brown color stool = 1 | 1 %-5 %weight loss = 1 |
| Very soft = 2 | Reddish color stool = 2 | 5 %-10 %weight loss = 2 |
| Watery = 3 | Bloody stool = 3 | 10 %–15 % weight loss = 3 |
| | | >15 %weight loss = 4 |

characterization.

#### 2.6.6. Therapeutic effect against IBD model

In terms of colitis treatment effect, BALB/c mice were randomly divided into four groups (n = 5 per group).

1 Control group: $H_2O$ + PBS
2 DSS group: 4 % DSS + PBS
3 Treat 1 group: 4 % DSS + Ce12@CD NPs (5 mg/kg)
4 Treat 2 group: 4 % DSS + Ce12@CD NPs (10 mg/kg)

The model of colitis was established by the continuous administration of 4 % DSS (w/v) on the 0~7th day, which was then replaced by drinking water on the following 8–16 days.

Mice in the DSS group, treat 1 group and treat 2 group were fed a 4 % DSS solution for 7 days to induce colitis and then switched to drinking water afterwards. On the 7th, 9th, 11th, and 13th days, the control group and DSS group were injected with PBS, while treat 1 group and treat 2 group received tail vein injections of Ce12@CD NPs at doses of 5 mg/kg and 10 mg/kg, respectively. The mice were euthanized on the 16th day. Body weight changes, fecal consistency and fecal bleeding of the mice were recorded daily over a 16-day period and the Disease Activity Index (DAI) was assessed according to the evaluation criteria in Table 1. In addition, in order to avoid environmental effects on the inflamed colon during sampling on day 16, one randomly selected colon from each group with different treatments was immediately taken for immunohistological characterization.

#### 2.6.7. mRNA sequencing and analysis

After treatment the colitis of different groups mice, the colons were collected for transcriptomic analysis on day 16 after treatment. BALB/c mice were divided into four groups (n = 3).

1 Control group: $H_2O$ + PBS
2 DSS group: 4 % DSS + PBS
3 Treat 1 group: 4 % DSS + Ce12@CD NPs (5 mg/kg)
4 Treat 2 group: 4 % DSS + Ce12@CD NPs (10 mg/kg)

Total RNA was extracted using the TRIzol reagent (Invitrogen, CA, USA) according to the manufacturer's protocol. RNA purity and quantification were evaluated using the NanoDrop 2000 spectrophotometer (Thermo Scientific, USA). RNA integrity was assessed using the Agilent 2100 Bioanalyzer (Agilent Technologies, Santa Clara, CA, USA). Then the libraries were constructed using VAHTS Universal V6 RNA-seq Library Prep Kit according to the manufacturer's instructions. The transcriptome sequencing and analysis were conducted by OE Biotech Co., Ltd. (Shanghai, China). The libraries were sequenced on a llumina Novaseq 6000 platform and 150 bp paired-end reads were generated. The clean reads were mapped to the reference genome using HISAT2. FPKM of each gene was calculated and the read counts of each gene were obtained by HTSeq-count. PCA analysis were performed using R (v 3.2.0) to evaluate the biological duplication of samples. Differential expression analysis was performed using the DESeq2. Q value $< 0.05$ and foldchange $>2$ or foldchange $<0.5$ was set as the threshold for significantly differential expression gene (DEGs). Based on the hypergeometric distribution, GO, KEGG pathway enrichment analysis of DEGs were performed to screen the significant enriched term using R (v 3.2.0), respectively. We utilized the KEGG or GO database for Gene Set Enrichment Analysis (GSEA).

#### 2.6.8. Gut microbiota 16S sequencing assay

Analysis of the microbiome. After different treatments of DSS induced colitis mice, the feces were harvested, frozen in liquid nitrogen immediately, and sent to Shanghai OE Biotech Co., Ltd for intestinal microbiome analysis by 16S sequencing method.

In terms of colitis treatment effect, BALB/c mice were divided into four groups (n = 5).

1 Control group: $H_2O$ + PBS
2 DSS group: 4 % DSS + PBS
3 Treat 1 group: 4 % DSS + Ce12@CD NPs (5 mg/kg)
4 Treat 2 group: 4 % DSS + Ce12@CD NPs (10 mg/kg)

Total genomic DNA was extracted using MagPure Soil DNA LQ Kit (Magan) following the Manufacturer's instructions. DNA concentration and integrity were measured with NanoDrop 2000 (Thermo Fisher Scientific, USA) and agarose gel electrophoresis. The bacterial 16S rRNA (V3–V4 region) genes were amplified with PCR using primers 343F (5′-TACGGRAGGCAGCAG-3′) and 798R (5′-AGGGTATCTAATCCT-3′). The Amplicon quality was visualized using agarose gel electrophoresis. Raw sequencing data were in FASTQ format. Paired-end reads were then preprocessed using Cutadapt software to detect and cut off the adapter. After trimming, paired-end reads were filtering low quality sequences, denoised, merged and detect and cut off the chimera reads using DADA2 with the default parameters of QIIME2. At last, the software output the representative reads and the ASV abundance table. Alpha diversity was measured based on the observed ASV number and presented with Chao, shannon and Simpson indices, based on the calculation of diversity index of different samples under the unified depth. Beta diversity was determined by principal coordinate analysis (PCoA) based on the distance matrix. The linear discriminant analysis effect size (LEfSe) method was used to compare the taxonomy abundance spectrum.

### 2.7. Statistical analysis

All data are presented as mean ± SEM. Comparison between groups was performed by one-way ANOVA analysis. NS, no significance; *$p < 0.05$, **$p < 0.01$, ***$p < 0.001$ and ****$P < 0.0001$ were considered to be statistically significant.

### 2.8. Data availability

The RNA sequencing data and 16S rRNA sequencing data generated in this study are deposited in the NCBI Sequence Read Archive (SRA). Their SRA data under BioProject accession numbers PRJNA1172615 and PRJNA1177412, and can be accessible with the links https://www.ncbi.nlm.nih.gov/sra/PRJNA1172615 and https://www.ncbi.nlm.nih.gov/sra/PRJNA1177412, respectively. The authors declare that all other data supporting the findings of this study are within the article or Supplementary Information file. Source data are provided with this paper.

## 3. Results and discussion

### 3.1. Preparation and characterization of Ce12@CD NPs

Ce6 ($Ce_6(\mu_3\text{-}O)_8(\mu_3\text{-}OH)_4(\mu_2\text{-}NH_2CH_2COO)_{10}$) was synthesized by a reaction between glycine and cerium (IV) nitrate in saturated sodium chloride solution at room temperature [28]. Using this Ce6 cluster as precursor to react with 1-adamantanecarboxylic acid (HADA) in N, N-Dimethylformamide at 85 °C, a new cerium cluster Ce12 with a formula of $[Ce_{12}(\mu_3\text{-}O)_8(\mu_3\text{-}OH)_8(\mu_2\text{-}OH)_6(ADA)_{18}]\bullet 3H_2O\bullet 3CH_3CN$ (Ce12)

was obtained. As shown in Fig. 1a, Crystallographic structure analysis revealed that Ce12 crystallizes in the cubic space group $P6_3/m$ and contains two $Ce^{4+}$ ions, three deprotonated $ADA^{-1}$ ligands, 8/6 $\mu_3$-O, 8/6 $\mu_3$-OH, one $\mu_2$-OH and one acetonitrile and one water molecules in its asymmetric unit. The whole skeleton of Ce12 is made up by a dumbbell-shaped $\{Ce_{12}\}$ metal-oxo core and 18 $ADA^{-1}$ ligands. This dumbbell-shaped $\{Ce_{12}\}$ metal-oxo core contains two equivalent octahedron-shaped $\{Ce_6\}$ metal-oxo core, which connect together by six $\mu_2$-OH bridges. Each $Ce^{4+}$ ion in the $\{Ce_{12}\}$ metal-oxo core is coordinated with eight O atoms, forming a square-antiprismatic coordination geometry. Adjacent $Ce^{4+}$ ions are connected together by the $\mu_3$-O, $\mu_3$-OH, and $\mu_2$-OH bridges. The outer coordination space of this $\{Ce_{12}\}$ metal-oxo core is surrounded by 18 deprotonated $ADA^{-1}$ ligands. Notably, these $ADA^{-1}$ ligands have large hydrophobic adamantine groups, thus this $\{Ce_{12}\}$ metal-oxo core center is located in a hydrophobic coordination environment, which may make this compound have low solubility while high stability in aqueous solution.

To enhance water solubility for further biological applications, we employed a host-guest driven self-assembly process between the adamantane moiety of Ce12 and β-cyclodextrin (β-CD) [29,30]. This improvement was validated *via* successful synthesis of Ce12@CD NPs, as confirmed by FT-IR spectroscopy (Fig. 1b). The hydroxyl (O-H) stretching vibration peak of pure β-CD is located at 3397 $cm^{-1}$, which is at 3441 $cm^{-1}$ in the spectrum of Ce12 attributed to the crystal water [31]. The spectral characteristics of the physical mixture (Ce12+β-CD) resembles that of pure β-CD, featuring a broad band at 3395 $cm^{-1}$. In contrast, the spectrum of Ce12@CD NPs exhibits a shift to a higher frequency at 3422 $cm^{-1}$. When comparing Ce12@CD NPs with Ce12, the O-H stretching vibration peak shifts 19 $cm^{-1}$ lower, indicating the formation of intermolecular hydrogen bonds between β-CD and Ce12 [32]. In the FT-IR spectrum of β-CD, peaks at 2927 $cm^{-1}$, 1156 $cm^{-1}$ and 1029 $cm^{-1}$ are attributed to the stretching vibrations of C-H, C-O-C, C-O respectively [33]. The Ce12 spectrum displays sharp peaks at 2903 $cm^{-1}$ and 2848 $cm^{-1}$ corresponding to the C-H stretching vibrations, which become weaker in the Ce12@CD NPs. This change suggested an interaction between adamantane and β-CD. The decreased intensity in absorption across various stretching and bending vibration modes evidences the interaction between Ce12 and the hydroxyl group at the

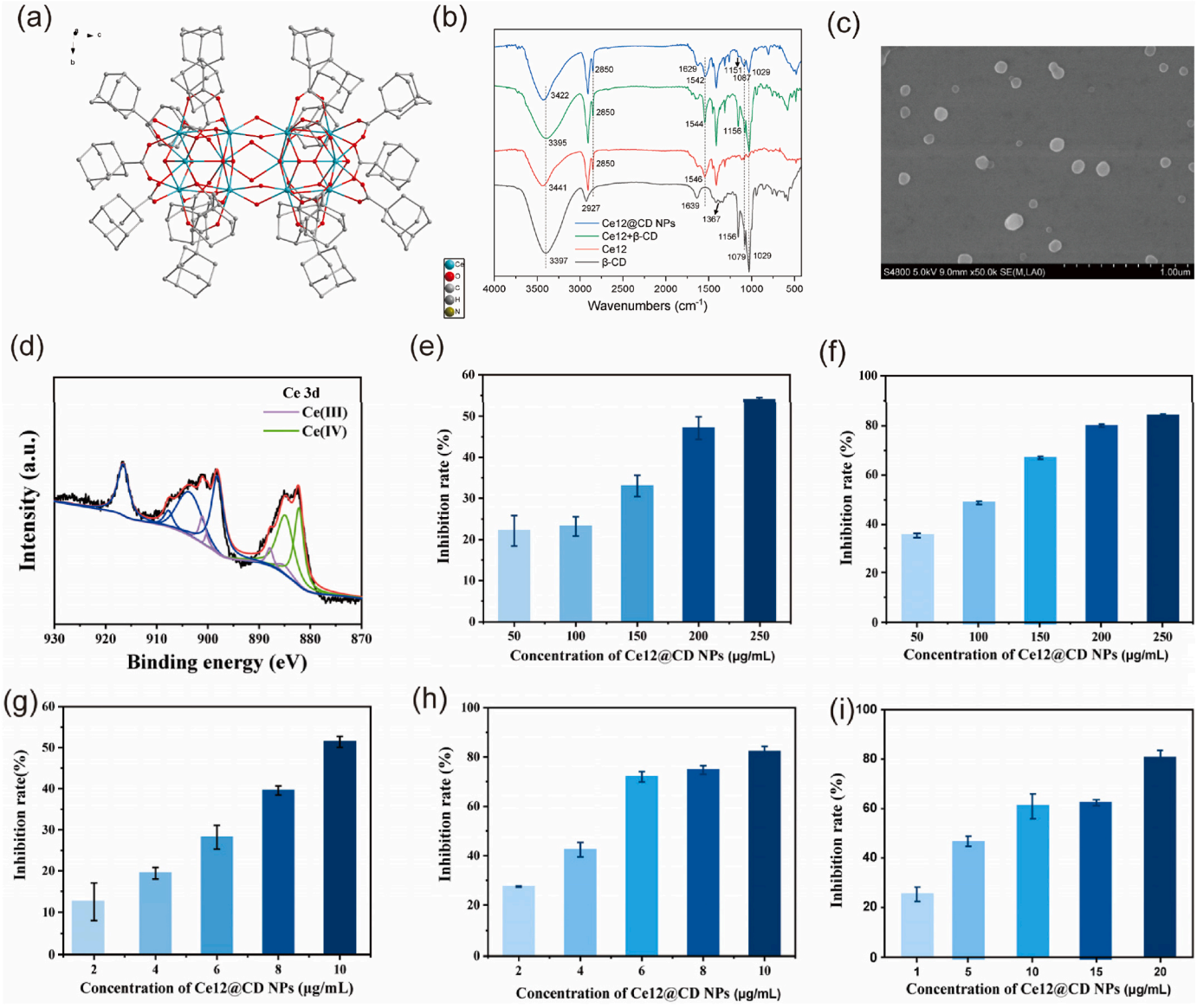


**Fig. 1.** Physical characterizations and RONS scavenging activity of Ce12@CD NPs. (a) Structure of Ce12 (X-ray single-crystal diffraction analysis image); (b) FT-IR spectra of β-cyclodextrin (β-CD), Ce12, their physical mix (Ce12 + β-CD) and Ce12@CD NPs; (c) SEM image of Ce12@CD NPs; (d) XPS analysis of Ce12@CD NPs; The antioxidant capacities of Ce12@CD NPs: (e) $H_2O_2$, (f) ·OH, (g) $O_2^{-}$·, (h) $ABTS^{+}$· and (i) DPPH· at various concentrations.

edge of the β-CD cavity, forming an inclusion compound [34]. Furthermore, the spectra comparison of β-CD and Ce12, Ce12@CD NPs reveals that the latter more closely resembles the spectrum of β-CD than that of Ce12, suggesting Ce12's encapsulation within the β-CD cavity [35]. Moreover, the SEM image reveals an octahedral Ce12 structure. Elemental mapping analysis further confirms the uniform distribution of C, O, and Ce elements within the Ce12 with typical signals (Fig. S1). XRD patterns of Ce12 and Ce12@CD NPs indicated that the crystalline structure of Ce12 remained stable during the process of self-assembly with β-CD (Fig. S2a).

Ce12@CD NPs had a diameter of around 51 nm (Fig. S2b) and a zeta potential of approximately −13.5 mV (Fig. S2c), as determined by dynamic light scattering (DLS). The Scanning Electron Microscope (SEM) revealed that the Ce12@CD NPs were uniform in shape, appearing as spherical particles (Fig. 1c). Spherical Ce12@CD NPs exhibit a relatively large specific surface area, which provides abundant surface-active sites for antioxidant reactions. This promotes the conversion of $Ce^{3+}/Ce^{4+}$ oxidation-reduction pairs, thereby enhancing their antioxidant performance. Spherical Ce12@CD NPs, with their high density of surface defects and oxygen vacancies, promote oxygen adsorption, activation, and release, boosting catalytic performance. Their nanoscale size contributes to high surface energy, which renders the surface atoms relatively unstable and enhances their reactivity. Concurrently, the diameter of Ce12@CD NPs was monitored over an seven-day period in water, PBS, phosphate buffer solutions (pH = 5.2, 6.5, and 7.4), and DMEM supplemented with 10 % serum using DLS. (Fig. S2d). The particle size remained largely unchanged, indicating the robust stability of Ce12@CD NPs. X-ray photoelectron spectroscopy (XPS) investigations of Ce12 and Ce12@CD NPs has confirmed the valence states of cerium. Fig. 1d indicated mixed valence +4 and + 3 in Ce12@CD NPs, whereas Ce12 revealed solely the +4 oxidation state (Fig. S2e). Ce12@CD NPs existed in both +3 and + 4 valence states, attributed to the higher surface-to-volume ratio that promotes $Ce^{3+}$ binding and facilitates the oxidation of solubilized oxygen in aqueous media [36]. The peaks around 901.23 eV and 885.36 eV for Ce $3d_{3/2}$ and Ce $3d_{5/2}$, respectively, are associated with $Ce^{3+}$ ions. Meanwhile, the characteristic XPS ($3d_{3/2}$) peak at 916.0 eV represents the transition of $Ce^{4+}$ ions from the initial state $3d^{10}4f^0$ to $3d^94f^0$ [37,38]. The $Ce^{3+}$ and $Ce^{4+}$ co-exist on the surface of Ce12@CD NPs with 11.58 % $Ce^{3+}$ determined by XPS analysis, providing the chemical basis for the catalytic activities to eliminate RONS [39,40].

### 3.2. RONS scavenging activity of Ce12@CD NPs

Given the presence of both $Ce^{3+}$ and $Ce^{4+}$ in Ce12@CD NPs, we investigated their scavenging activity against RONS using various colorimetric assays. Initially, three representative ROSs, namely, Hydrogen peroxide ($H_2O_2$), superoxide anions ($O_2^{-}\cdot$), and hydroxyl radicals (·OH) were selected to evaluate the ROS scavenging capabilities of Ce12@CD NPs using corresponding assay kits respectively. Approximately 54 % of the total $H_2O_2$ and 83 % of ·OH were removed by 250 μg/mL of Ce12@CD NPs (Fig. 1e and f). Additionally, around half of the $O_2^{-}\cdot$ was decomposed when treated with 10 μg/mL of Ce12@CD NPs (Fig. 1g). Furthermore, we investigated the antioxidative properties of Ce12@CD NPs by examining their ability to scavenge reactive nitrogen species (RNS) using two distinct assays: 2,2′-azino-bis (3-ethylbenzothiazoline 6-sulfonate) (ABTS) and 2,2-di-(4-tert-octylphenyl)− 1-picrylhydrazyl (DPPH), as determined by the reduction in solution absorbance at wavelengths of 414 nm and 517 nm, respectively. Notably, at relatively low concentrations (10 and 20 μg/mL), Ce12@CD NPs exhibited more than 80 % clearance of $ABTS^{+}\cdot$ and DPPH·, demonstrating their effectively scavenging of free radicals and total RNS, respectively (Fig. 1h and i). Importantly, the scavenging of RONS by Ce12@CD NPs was dose-dependent, highlighting their broad-spectrum free radical scavenging capability to eliminate RONS.

To pinpoint the detailed performances of Ce12@CD NPs, we examine their CAT- and SOD-like activity. The generation of oxygen in a concentration-dependent manner when $H_2O_2$ solution was exposed to Ce12@CD NPs indicated their CAT-like enzymatic activity (Fig. S2f). Additionally, the SOD-like enzyme activity of Ce12@CD NPs was confirmed by the decrease in absorbance at 560 nm with increasing Ce12@CD NPs concentration (0–20 μg/mL), as assessed using the SOD enzyme assay kit (Fig. S2g).

Since the CAT-mimetic activity of Ce12@CD NPs, which could catalyze the conversion of $H_2O_2$ into $H_2O$ and $O_2$, and RNS scavenging activity have been known to be related to the $Ce^{4+}$ fraction on the surface. And the $Ce^{3+}$ sites are responsible for eliminating ·OH and $O_2^{-}\cdot$ *via* redox reactions or SOD-mimetic activity [41,42]. The facile electron shuttling and regeneratable changes between $Ce^{3+}$ and $Ce^{4+}$ on Ce12@CD NPs promote the scavenging reactions for RONS, as well as antioxidant and catalytic properties.

### 3.3. ROS scavenge and cell protection of Ce12@CD NPs in vitro

Due to the excellent RONS clearance activity of Ce12@CD NPs, we further evaluated the cellular ROS clearance and protection effects on lipopolysaccharide (LPS)-/$H_2O_2$-induced HUVEC or RAW264.7 macrophages. Initially, we assessed the biosafety of different concentrations of Ce12@CD NPs on HUVEC and RAW264.7 macrophages using the MTT assay. Even after being exposed to a concentration of 200 μg/mL for 24 h, the cell viability of HUVEC and RAW264.7 cells was as high as 90.42 ± 3.10 % and 86.12 ± 4.84 %, respectively (Fig. S3a). These results indicate minimal cytotoxicity and no significant adverse effects on the cells. Hemolysis tests also demonstrated excellent blood compatibility, with a hemolysis rate dispersion of less than 3 % for all concentrations of Ce12@CD NPs (Fig. S3b). Since oxidative stress injury is associated with elevated levels of $H_2O_2$ [43], we established a nutrient stress environment in the cells by incubating them with 1 mM $H_2O_2$. To assess the *in vitro* antioxidant activity of Ce12@CD NPs, we used 2′,7′-Dichlorodihydrofluorescein diacetate (DCFH-DA) as the oxidant-sensing probe to detect ROS generation and clearance using confocal laser scanning microscope (CLSM). In the presence of ROS, DCFH-DA is oxidized to green fluorescent 2′, 7′-dichlorofluorescein (DCF). As shown in Fig. 2a, the fluorescent intensity of DCF in cells treated with combination of Ce12@CD NPs and $H_2O_2$ was lower compared to the $H_2O_2$ group, suggesting that Ce12@CD NPs possessed dose-dependent antioxidant property in HUVEC cells. Notably, HUVEC cells treated with 100 μg/mL Ce12@CD NPs showed no significant difference compared to control cells. Due to their potent ROS scavenging activity, Ce12@CD NPs effectively protect cells from ROS-mediated cytotoxicity.

Furthermore, macrophages play a crucial role in the development of oxidative stress and inflammatory diseases. To investigate the potential anti-inflammatory activity of Ce12@CD NPs, we examined their protective effect against LPS-induced injury in RAW264.7 macrophages and measured the levels of several key pro-inflammatory cytokines such as tumor necrosis factor-α (TNF-α), interleukin-6 (IL-6) and interleukin-1β (IL-1β). After inducing RAW264.7 macrophages with LPS, IL-1β increased by 4 times (Fig. 2b), TNF-α increased by 2 times (Fig. 2c) and IL-6 increased by about 0.6 times (Fig. 2d). Treatment with Ce12@CD NPs alleviated the oxidative stress of RAW264.7 macrophages, as indicated by DCFH-DA (Fig. S3c), and down-regulated the expression of proinflammatory cytokines IL-1β, TNF-α and IL-6 (Fig. 2b–d), showing a significant concentration dependent effect. Specially, at a concentration of 100 μg/mL Ce12@CD NPs, there are significant down-regulation rates observed for IL-1β (58.37 %), TNF-α (51.50 %), and IL-6 (35.22 %), respectively. These results suggested that Ce12@CD NPs can effectively eliminate toxic ROS to reduce the level of pro-inflammatory cytokines in RAW264.7, and have a beneficial effect on inflammation resolution. The ROS-scavenging capability of Ce12@CD NPs, coupled with their multi-enzyme activity, protects cells from oxidative stress-induced damage, indicating their potential in therapy for IBD.

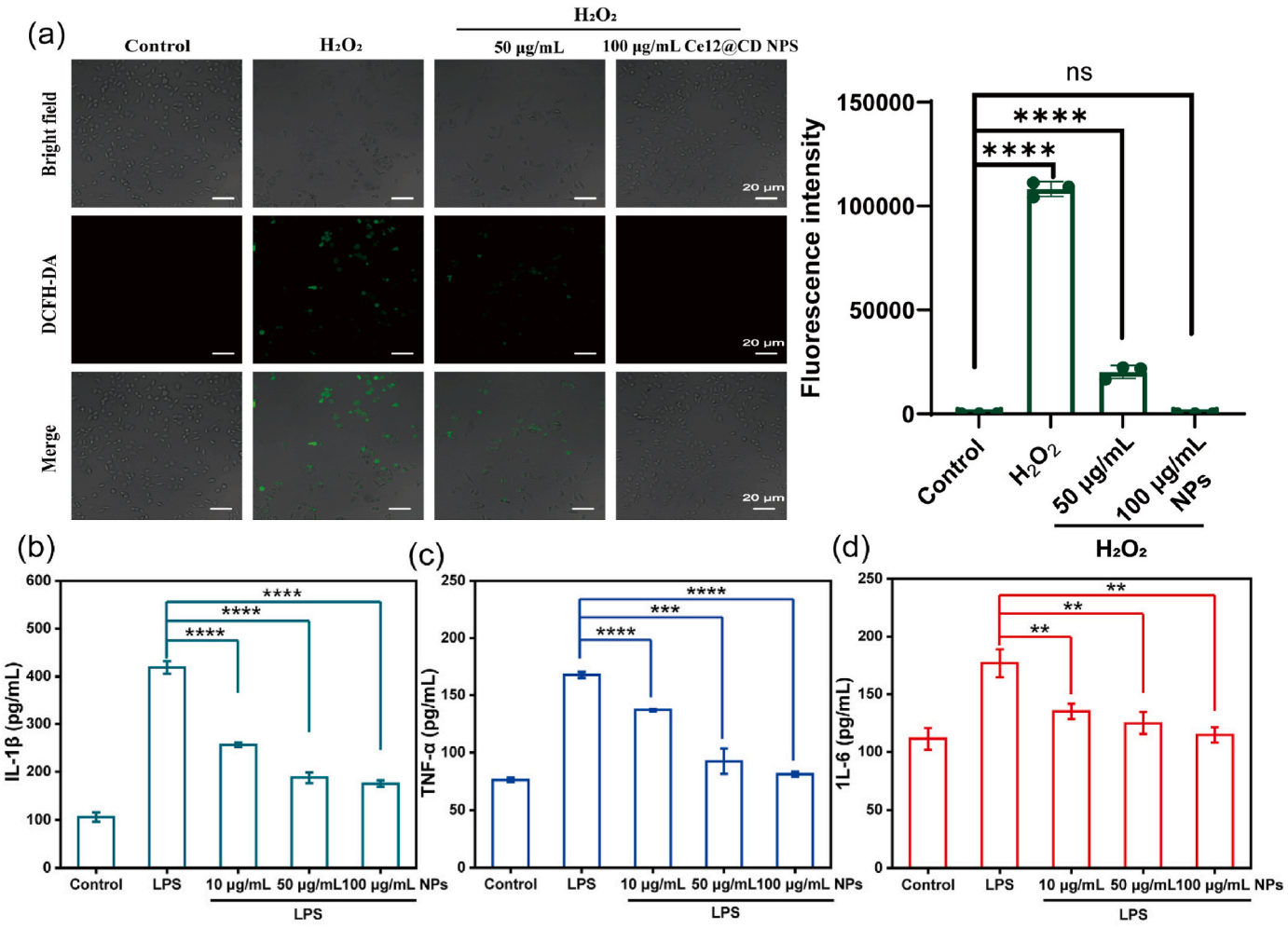


**Fig. 2.** Protective effects of Ce12@CD NPs cells *in vitro*. (a) CLSM images (Left) and statistical analysis (Right) probed by DCFH-DA in HUVEC cells untreated, treated with $H_2O_2$, or with $H_2O_2$+Ce12@CD NPs at varying concentrations (scale bar: 20 μm); (b–d) The levels of proinflammatory factors in RAW264.7 macrophages after different treatments, including (b) IL-1β, (c) TNF-α, and (d) IL-6.

### *3.4. Therapeutic and prophylactic effects of Ce12@CD NPs on DSS-induced inflammatory bowel disease*

The excessive formation of RONS at the colonic site is a prominent feature of IBD. Based on the *ex vivo* antioxidant and anti-inflammatory effects, the therapeutic and prophylactic efficacy of Ce12@CD NPs against colitis *in vivo* was evaluated. Prior to this, we assessed their biocompatibility, distribution and pharmacokinetics profile in healthy mice (Fig. S4a). The results of blood routine examination, blood biochemical analysis, and HE staining showed almost no significant difference from those of healthy mice (Fig. S4b-4d), indicating that treatment with 10 mg/kg Ce12@CD NPs did not compromise major organs health or functionality, indicating good biocompatibility *in vivo*. Large amounts of Ce12@CD NPs were distributed to major organs *via* the circulation, with the highest accumulation in the liver by 22.09 ± 1.63 % ID/g at 6 h, decreasing to about 2.9 ± 1.0 % ID/g at 24 h (Fig. S4e). This suggests elimination of Ce12@CD NPs *via* hepatobiliary metabolism, allowing for rapid clearance into the circulation without causing obvious adverse effects. The blood pharmacokinetics of Ce12@CD NPs followed a typical one-compartment model, with a blood clearance half-life of 2.20 h, indicating moderate blood elimination *in vivo* (Fig. S4f). We also collected a portion of feces and urine daily, and after one week, the accumulated Ce contents were 28.76 and 19.26 μg and the Ce contents in feces and urine decreased by 78.79 ± 0.91 % and 73.80 ± 0.85 %, respectively, suggesting that Ce12@CD NPs could be excreted *via* the kidney and hepatointestinal systems (Fig. S4g). Effective metabolism of Ce12@CD NPs resulted in their elimination from the body within one week without long-term toxicity, ensuring the safety of Ce12@CD NPs for IBD treatment.

To investigate the therapeutic efficacy Ce12@CD NPs of against IBDs, we constructed DSS-induced colitis model by giving 4 % DSS (w/v) to mice over a 7-day period before administering Ce12@CD NPs intravenously every 2 days for 7 days (Fig. 3a). The control groups included mice without DSS treatment and those treated with PBS (The healthy control group), as well as mice with DSS treatment and those treated with PBS (The colitis control group). The colitis mice exhibited significant weight loss and an increase in the disease activity index (DAI) scores, accompanied by severe diarrhea, bloody stool, and other symptoms, these findings indicate the successful establishment of the colitis mouse model. The feces of the Control group mice were characterized by firm, dark brown, regularly shaped oval pellets. In contrast, the feces of the DSS group mice were unformed, with visible bright red blood and increased adhesion, often adhering to the upper part of the EP tube. Following treatment with Ce12@CD NPs, the hardness and texture of the feces were restored to levels comparable to those of the Control group, particularly in the high-dose Treat 2 group (Fig. S5).

The body mass of mice in the colitis control group dropped sharply to 78.88 ± 4.34 % of the initial weight by day 16 (Fig. 3b), and their DAI score reached 8.6 ± 0.89 (Fig. 3c). In contrast, in the groups treated with 5 mg/kg and 10 mg/kg Ce12@CD NPs, the mice's body weight initially

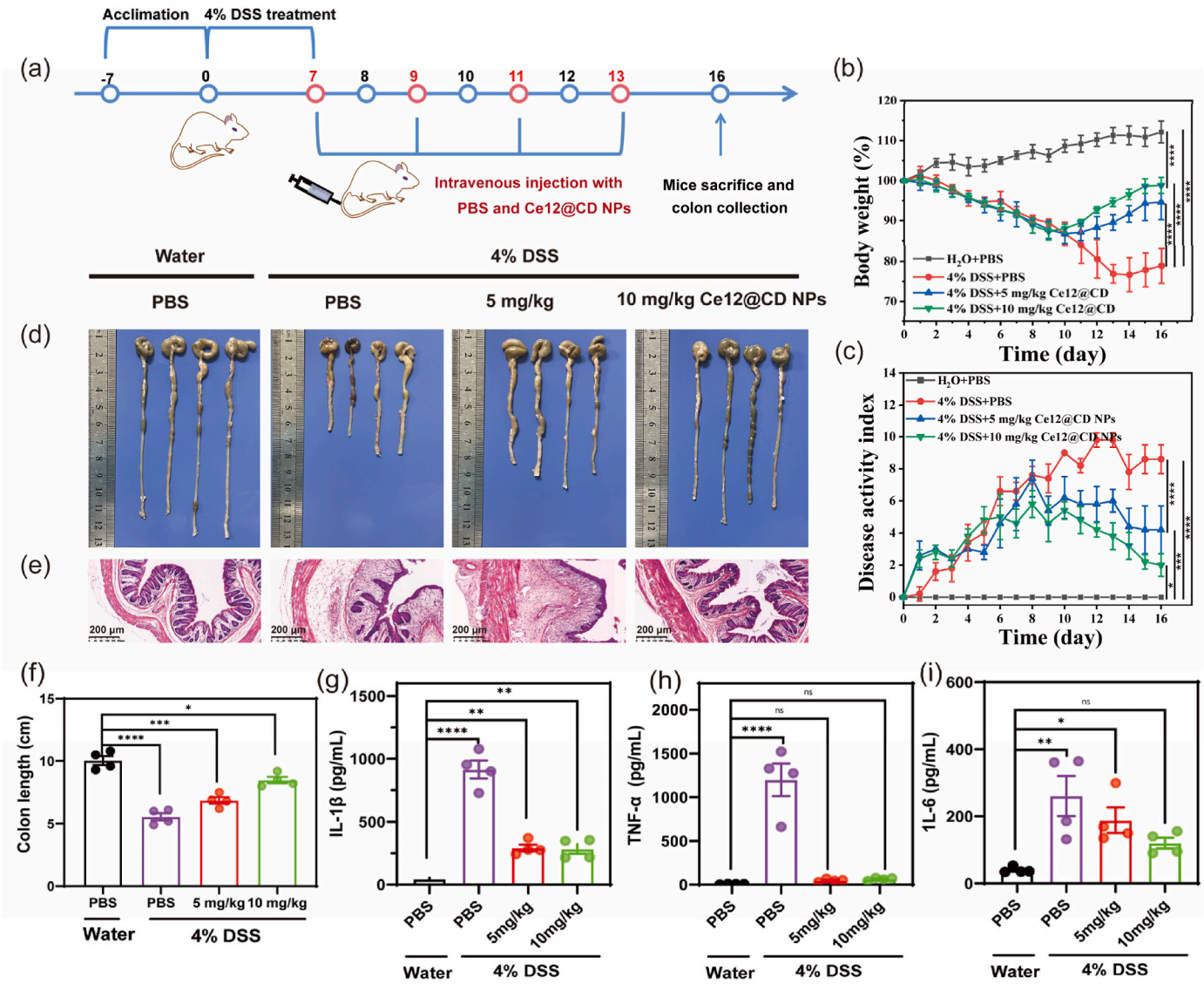


**Fig. 3.** Therapeutic effect of Ce12@CD NPs administered intravenously on DSS-induced colitis. (a) Experimental schematic for DSS-induced colitis and therapeutic administration of Ce12@CD NPs; (b) The daily changes in body weight and (c) DAI assessment of the mice during a 16-day treatment course. (d) Digital photographs showcasing the colon, along with (e) H&E staining of colon tissue sections (Scale bar: 200 μm), and (f) corresponding measurements of colon lengths for each group. (g–i) quantitative analysis of pro-inflammatory factors (IL-1β, TNF-α, and IL-6) in the colon tissue. *p < 0.05, **p < 0.01.

decreased and then increased from day 8–16, finally reaching 94.58 ± 4.33 % and 98.84 ± 1.97 % of the initial weight, respectively, while the DAI score reduced to 4.2 ± 1.48 and 2.0 ± 0.71, respectively. The detrimental inflammatory reactions triggered by colitis can also causes a shortening of colon length due to intestinal mucosa damage. Therefore, the colons of mice were isolated, imaged and measured when the mice were sacrificed at Day 16 (Fig. 3d). In contrast to the colon length of healthy control mice (10.05 ± 0.71 cm), colitis control mice had a significantly shorter colon length of only 5.55 ± 0.59 cm. However, the colon length of mice treated with 10 mg/kg Ce12@CD NPs significantly increased to 8.48 ± 0.52 cm (Fig. 3f). These quantitative data demonstrate that Ce12@CD NPs provided symptomatic relief of colitis symptoms, indicating the restoration of the mice's health after treatment. H&E staining of colon tissues showed significant destruction of colon microstructure, the loss of crypts, destruction of goblet cells and immune cells infiltration were observed in colitis mice, while no significant tissue damage was observed in healthy mice and 10 mg/kg Ce12@CD NPs treated mice (Fig. 3e). This suggests that Ce12@CD NPs can significantly alleviate the typical symptoms of colitis, and the therapeutic efficacy is enhanced at a dose of 10 mg/kg. Subsequently, we measured proinflammatory mediators in the colon tissue, including myeloperoxidase (MPO), SOD enzyme, TNF-α, IL-6, and IL-1β, which are known markers of IBD and contribute to its development. The activity of MPO enzyme can reflect the infiltration level of neutrophils, and the infiltration of a large number of recruited inflammatory cells caused by colitis leads to an increase in MPO enzyme activity. SOD enzyme is an antioxidant metalloenzyme present in organisms and scavenges free radicals. In colon tissues of colitis control group, the MPO enzyme activity increase to 1.43 ± 0.29 (U/mg tissue) and SOD enzyme activity was significantly reduced to 0.24 ± 0.36 (U/mg tissue), consistent with a previous report [44]. After 10 mg/kg Ce12@CD NPs treatment, the activities of MPO and SOD were significantly restored to normal levels of 0.11 ± 0.02 (U/mg tissue) and 1.25 ± 0.06 (U/mg tissue), respectively (Fig. S6a and Fig. S6b). Levels of the proinflammatory cytokines (TNF-α, IL-1β, and IL-6) in colon tissue homogenates were measured using enzyme-linked immunosorbent assay (ELISA) and immunofluorescence staining. As a result, the levels of TNF-α, IL-1β, and IL-6 significantly increased following DSS induction, which were normalized after 10 mg/kg Ce12@CD NPs treatment by 69 %, 95 % and 54 % reduction respectively. (Fig. 3g-I, Fig. S6c). In addition, the analysis of blood

routine parameters showed that they remained within the normal range after treatment (Fig. S6d). H&E staining revealed that Ce12@CD NPs induced no evident organ injuries or inflammatory lesions in vital organs such as heart, liver, spleen, lungs and kidneys (Fig. S6e). These results suggest that Ce12@CD NPs exerted excellent therapeutic potential in the colitis model without causing significant side effects.

Furthermore, we investigated the prophylactic efficacy of Ce12@CD NPs in protecting mice from colitis development. Mice were injected with PBS or Ce12@CD NPs (5 or 10 mg/kg) once every 2 days while simultaneously given DSS for the initial 7 days to induce colitis until they were euthanized on day 9. As shown in Fig. S7 and Fig. S8, Ce12@CD NPs dose-dependently displayed superior preventive efficacy against colitis, with regained lost weight, increased colon length, minimized colon injury, and decreased the levels of proinflammatory factors levels. Moreover, histological examination of primary organs and blood routine examination (Figs. S8a–8b) consistently indicated almost no apparent blood toxicity and no structure or pathological changes in mice treated with 10 mg/kg Ce12@CD NPs.

Together, Ce12@CD NPs exhibited robust therapeutic effects in both preventing and treating colitis, offering a promising drug for IBD.

### 3.5. RNA sequencing analysis of Ce12@CD NPs -treated mice colon

To elucidate the mechanisms underlying the anti-inflammatory effects of Ce12@CD NPs, colonic tissues from DSS-induced colitis mice treated with Ce12@CD NPs were subjected to RNA sequencing analysis. Mice were randomly allocated into 4 groups (n = 3): the control group representing healthy mice (Control), the DSS-induced colitis group (DSS), 5 mg/kg Ce12@CD NPs-treated group (Treat1), and 10 mg/kg Ce12@CD NPs-treated group (Treat2). Hierarchical clustering analysis (Figs. S9a and S9b) indicated that the gene expression profiles in 10 mg/kg Ce12@CD NPs-treated colitis mice showed trends towards those of healthy mice, however, they exhibited significant differences compared to DSS-induced colitis mice. A comparative analysis revealed 1450 differentially expressed genes (DEGs) between the DSS-treated and control groups, with 1156 and 268 DEGs identified at low and high concentrations of Ce12@CD NPs treatments, respectively (Fig. S10a). Additionally, a comparative gene expression analysis indicated that in the colons of DSS-induced colitis mice, 805 genes were upregulated and 645 genes downregulated when compared with the healthy controls. Post-treatment with Ce12@CD NPs (10 mg/kg), these figures were modified to 611 upregulated and 258 downregulated genes (Figs. S10a and S10b). As shown in Fig. 4a, in the comparison of up-regulated and down-regulated genes, there was an overlap of 489 genes and 207 genes between the two sets, respectively, which indicates Ce12@CD NPs treatment appears to mitigate some of the DSS-induced gene expression changes. Moreover, there were several genes, including Reg3a, Reg 3d, IL6 and csf3 that overlapped between the top 10 up-regulated and down-regulated genes in both the DSS group compared to the control group and in the DSS group versus the 10 mg/kg Ce12@CD NPs-treated group. This overlap could be attributed to inflammation (Figs. S9a and S9b).

The identified differentially expressed genes were subjected to clustering and enrichment analysis in order to elucidate the underlying therapeutic mechanism. Gene Ontology (GO) enrichment analysis revealed that Ce12@CD NPs (10 mg/kg) treatment intersected with various biological processes, including inflammatory response,

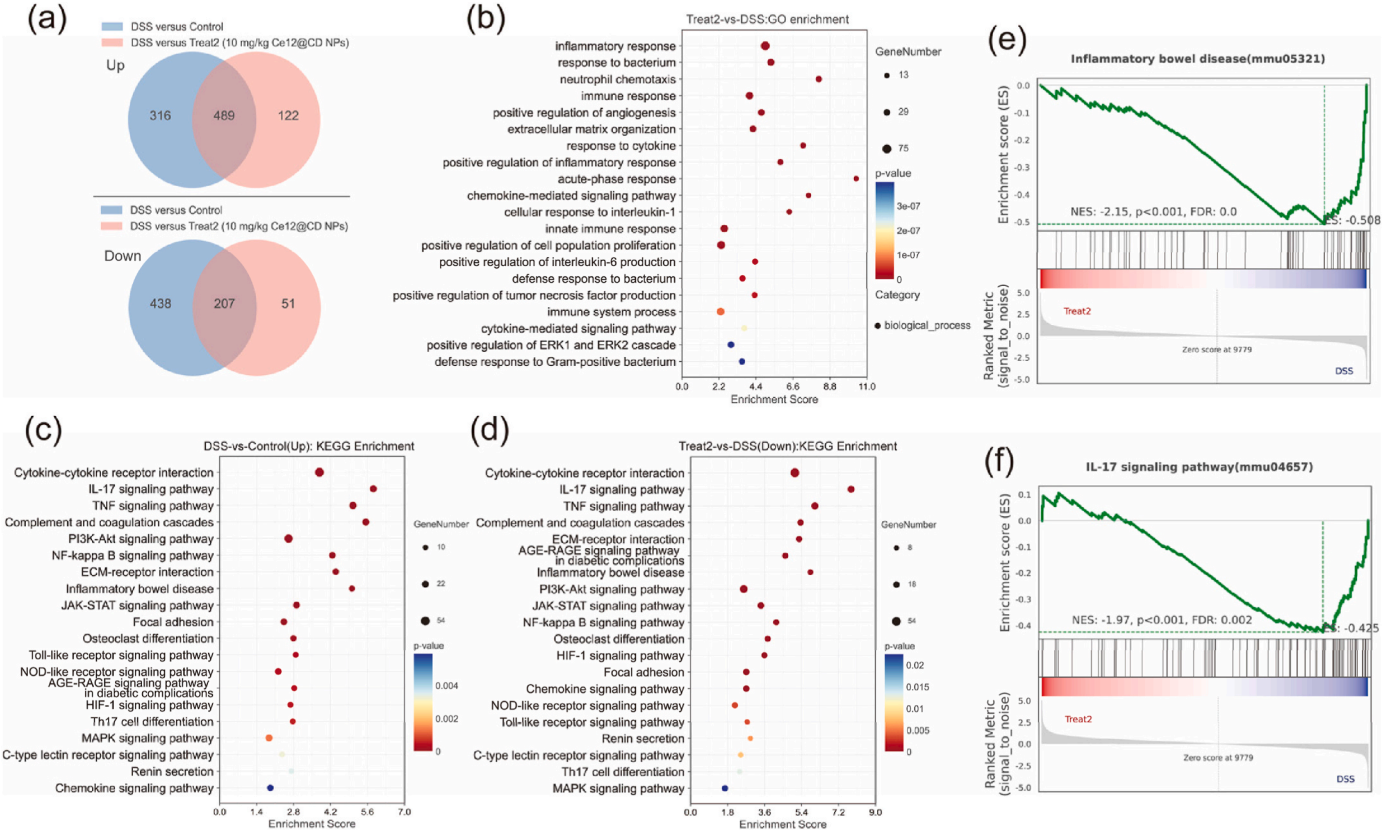


**Fig. 4.** Mechanism study of Ce12@CD NPs for IBD treatment by Transcriptomic profiles analysis. (a) Venn diagram of RNA-seq analysis showing significantly up-regulated (top) or down-regulated (bottom) genes in the DSS group compared to the control group and in the DSS group (DSS) versus the 10 mg/kg Ce12@CD NPs treated group (Treat2). (b) GO biological process clustering analysis in 10 mg/kg Ce12@CD NPs treated group versus the DSS group. KEGG pathways enriched the (c) up-regulated genes in the DSS group versus the control group and the (d) down-regulated genes in the 10 mg/kg Ce12@CD NPs treated group compared to DSS group. GSEA showed "genes expression difference of " (e) Inflammatory bowel disease and (f) IL-17 signaling pathway between 10 mg/kg Ce12@CD NPs group and DSS-induced colitis group (Fold Change $\geq$2 and P $<$ 0.05).

neutrophil chemotaxis, immune response, response to cytokine, response to bacterium, defense response to bacterium, epidermis development, response to oxidative stress, regulation of reactive oxygen species metabolic process, and more (Fig. 4b). Expression differences including inflammatory response, neutrophil chemotaxis, immune response, innate immune response, response to bacterium, epidermis development, response to oxidative stress, superoxide metabolic process and more were observed between the DSS-induced colitis group and the healthy control group (Fig. S11). These results lend support to the hypothesis that Ce12@CD NPs may have roles in modulating the inflammatory responses, potentially involving anti-inflammatory and immunomodulatory pathways, as well as ROS metabolism. Additionally, we can draw the hypothesis that Ce12@CD NPs has the potential to regulate gut bacteria, which also contribute to the treatment of colitis.

The protective action exerted by Ce12@CD NPs on the intestinal mucosal barrier and its inhibition of inflammatory responses could represent a critical biological pathway for the amelioration of colitis symptoms. Kyoto Encyclopedia of Genes and Genomes (KEGG) pathway enrichment analysis suggests downregulation of the IL-17 signaling, inflammatory bowel disease and TNF, PI3K/AKT NF-κB, JAK-STAT signaling pathways are highly associated with the therapeutic mechanisms of the Ce12@CD NPs (Fig. 4c and d). In DSS-treated mice, these pathways were abnormally activated, but their activity was significantly depressed following the intervention with Ce12@CD NPs. The KEGG enrichment analysis revealed that the IL-17 signaling pathway showed significant enrichment, suggesting it may be involved in the therapeutic effects of Ce12@CD NPs. IL-17 is considered one of the major pathogenic factors in IBD. Upon activation of the IL-17 signaling pathway, more pro-inflammatory cytokines such as TNF-α and IL-6 are released, thereby amplifying the inflammatory process.

Regarding the other enriched pathways, the TNF and NF-κB pathway are recognized as pivotal inflammatory pathway. PI3K-AKT and HIF-1 signaling pathway activation could trigger macrophage polarization toward the anti-inflammatory M2 phenotype [45]. Additionally, JAK/-STAT signaling pathway was report to be involved in both innate and adaptive immune response in IBD [46]. This analysis illuminates the substantial normalization of key gene expressions related to these signaling pathways in the colons of colitis mice following Ce12@CD NPs treatment.

Gene Set Enrichment Analysis (GSEA) further corroborated the downregulation of gene signatures associated with Inflammatory bowel disease (Fig. 4e), IL-17 signaling pathways (Fig. 4f) and TNF, NF-κB,

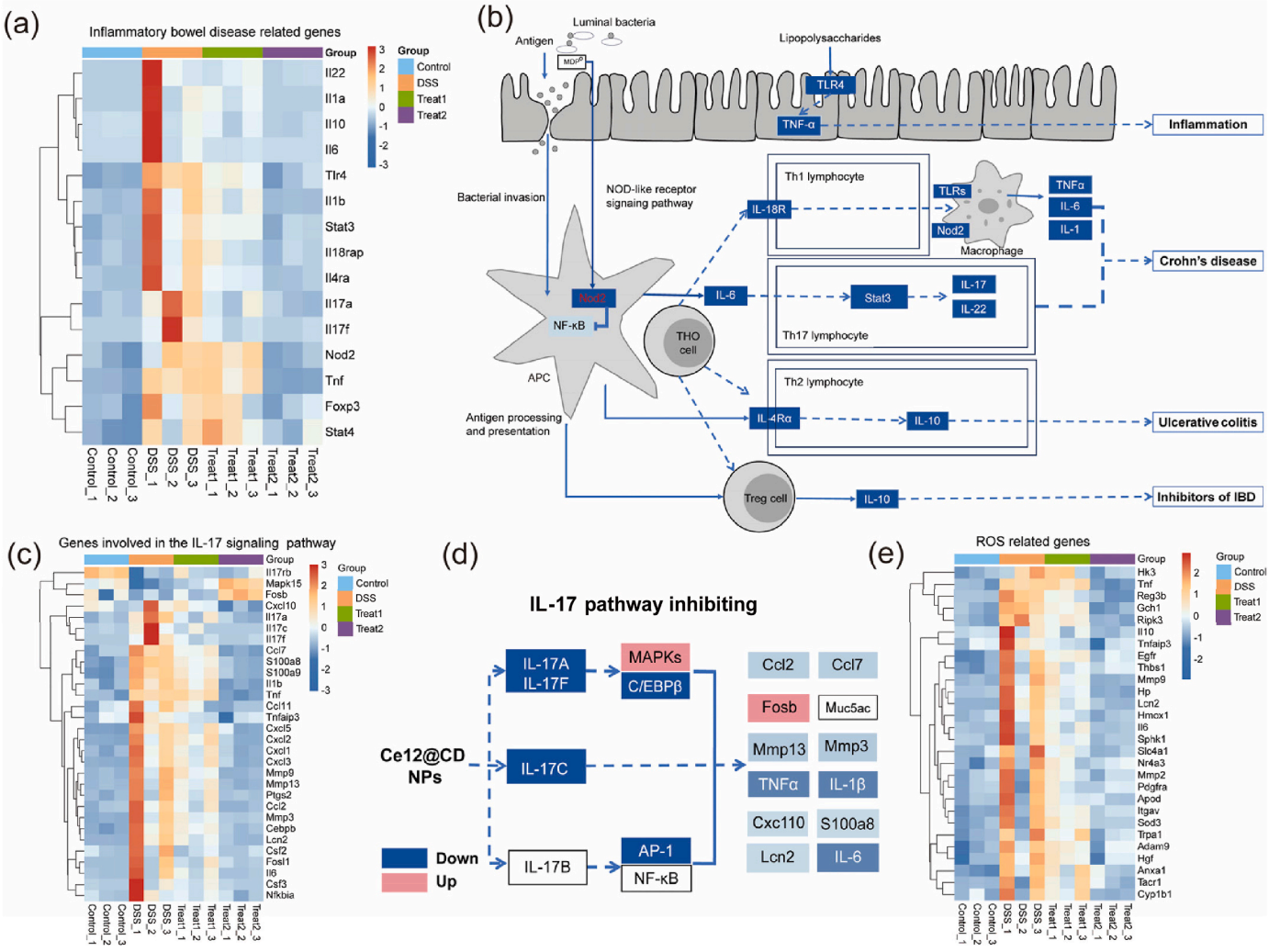


**Fig. 5.** Mechanism study of Ce12@CD NPs for IBD treatment by Transcriptomic profiles analysis. (a) Heatmap of significantly upregulated and downregulated gene expression involved in the "Inflammatory bowel disease"(Fold Change ≥2 and $P < 0.05$), along with (b) a schematic diagram showing differentially expressed genes in KEGG database between the Treat2 group and the DSS group. (c) Heatmap of significantly upregulated and downregulated gene expression involved in the "IL-17 signaling pathway"(Fold Change ≥2 and $P < 0.05$), along with (d) a schematic diagram showing differentially expressed genes in KEGG database between the Treat2 group and the DSS group. Up-regulated genes are marked with pink, down-regulated genes are marked with blue, white indicates both up-regulated and down-regulated genes. (e) Normalized heatmap displaying the response to ROS-related genes in the groups (Fold Change ≥2 and $P < 0.05$).

MAPK, JAK-STAT, HIF-1 signaling pathways in the Ce12@CD NPs-treated groups (Fig. S12). The MAPK pathway, recognized as a classic pro-inflammatory cascade, plays a critical role in governing lymphocyte influx into the gut in IBD patients [47]. Heatmaps (Fig. 5a) and schematic diagram (Fig. 5b) shown that inflammatory bowel disease related genes were significantly upregulated in the DSS group and downregulated in the Ce12@CD NPs-treated group, especially the higher concentrations of Ce12@CD NPs (10 mg/kg), respectively. As is shown in Fig. 5c and d, in both treatment concentrations of Ce12@CD NPs, the IL-17 signaling pathway was notably downregulated. The suppression of the IL-17 pathway leads to decreased AP-1 expression, which is crucial in regulating inflammation through the stimulation of key inflammatory mediators, specifically CXCL2, CXCL5, and IL-6. Of particular interest, the IL-17 signaling pathways showed more downregulation in the higher concentration group. We also applied GSEA methods based on GO enrichment analysis, which further confirming the significant correlation of various biological processes including inflammatory response, immune response, chemokine activity, cytokine activity, oxidoreductase activity, acting on paired donors, and cytochrome-c oxidase activity with Ce12@CD NPs treatment (Fig. S13). The up-regulation of oxidoreductase activity and acting on paired donors, and cytochrome-c oxidase activity may be related to the promotion of REDOX enzyme reaction by the antioxidant capacity of Ce12@CD NPs.

Therefore, by analyzing the detailed ROS-related gene expression,

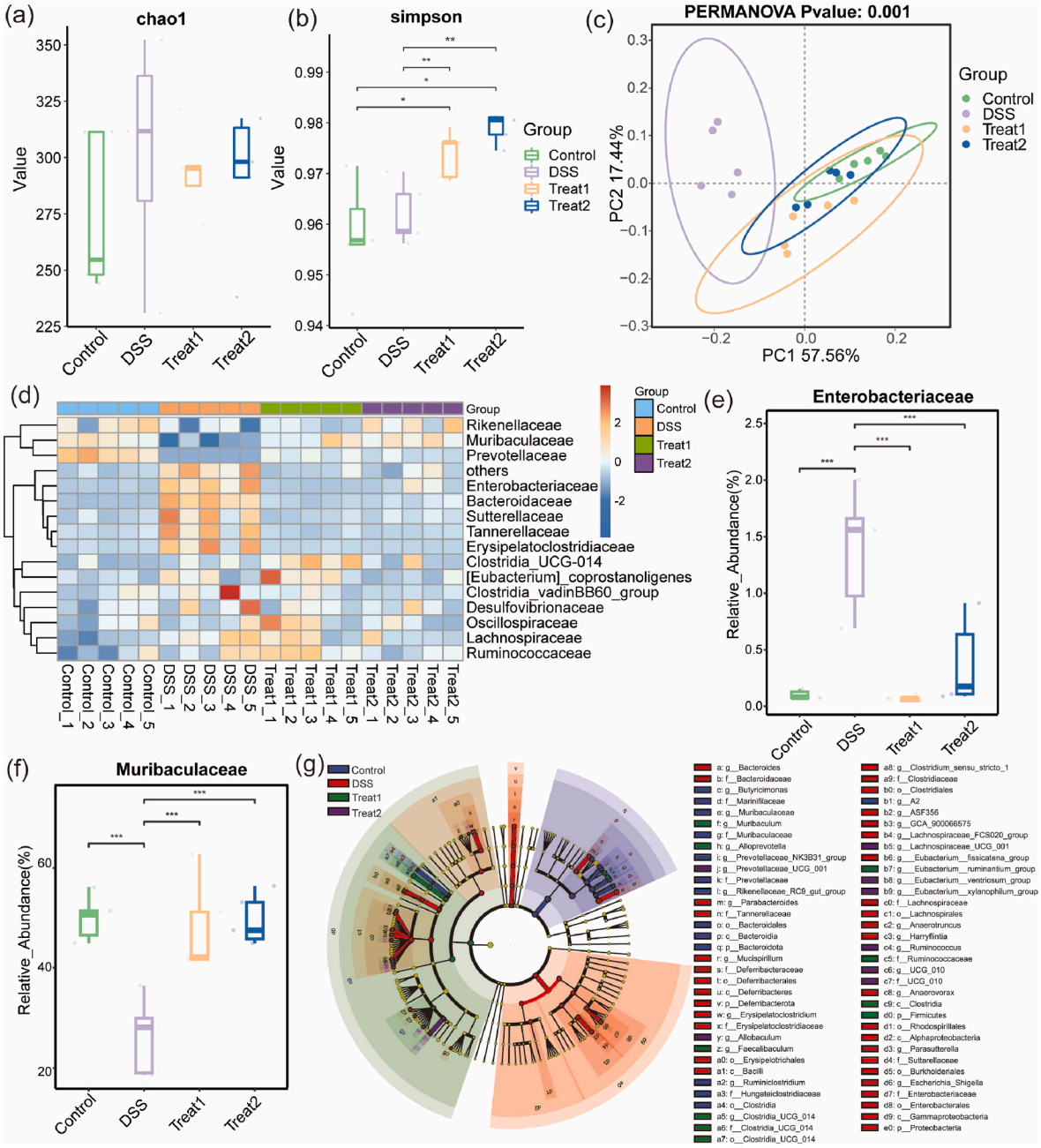


**Fig. 6.** Ce12@CD NPs treatment altered the gut microbiota diversity and composition. Alpha diversity estimated by the (a) Chao, and (b) Simpson indices of ASV level. (c) Principal coordinate analysis (PCoA) using Weighted Unifrac distances of beta diversity. (d) Heatmap illustration of gut microbial distribution at the Family level. Relative abundance of (e) Enterobacteriaceae and (f) Muribaculaceae. (g) Cladogram based on LEfSe analysis indicating the community composition of the gut flora. Each circle at different taxonomic levels represents a taxon at that level, and its diameter is proportional to the relative abundance n = 5 for each group. Statistical analysis was evaluated with one-way ANOVA (*P < 0.05, **P < 0.01, ***P < 0.001).

we found that the genes were active in DSS-treated group, However, after treatment with Ce12@CD NPs, there was a predominant decrease in the gene signature associated with response to ROS in colitis mice. (Fig. 5e). ROS could promote the elevation of pro-inflammatory cytokines like IL-1β, IL-6, and TNF-α [48]. TNF-α could trigger a strong cascade inflammatory response *via* the TNF-α/NF-κB signaling pathways, resulting in an uncontrolled inflammation response in colitis mice [49]. Consistently, the above findings demonstrate that the Ce12@CD NPs effectively mitigate colitis in mice through inhibiting the NF-κB and TNF signaling pathways through a reduction in ROS level.

What's more, differing concentrations of Ce12@CD NPs significantly dampened the inflammatory and immune responses with the higher concentration exhibiting a superior therapeutic effect, more effectively abating inflammation and mitigating immune responses (Fig. S14).

These findings suggest Ce12@CD NPs likely alleviates colitis in part by inhibiting inflammation-related signaling pathways, diminishing proinflammatory cytokines' levels and decreasing the ROS level.

### 3.6. Modulatory effect of Ce12@CD NPs on the gut microbiome

The excessive production of ROS in colitis will damage the intestinal mucosal barrier, leading to the invasion of intestinal bacteria and ultimately leading to dysbiosis of IBD. Similarly, the disruption in the gut microbiota membership and their metabolites has a significant influence on the initiation and progression of IBD [50]. To investigate whether Ce12@CD NPs can modulate the composition of commensal microbiota to maintain a balanced gut environment, we conducted microbial sequencing using 16S ribosomal RNA (rRNA) gene sequencing targeting the V3-V4 regions, this allowed us to assess diversity and identify the specific makeup of gut microbes. We can roughly see the degree of samples dispersion within the group and the differences in index values between different groups. As depicted in Fig. 6a, the Chao 1 alpha diversity analysis indicates that the gut microbiota composition of the groups treated with two concentrations of Ce12@CD NPs (Treat1 and Treat2) remained largely unchanged, exhibiting no significant deviation from that of the healthy control group. Notably, Ce12@CD NPs treatment was associated with changes in microbial diversity and community richness, indicating a potential positive impact as shown by analysis of α-diversity (Simpson (Fig. 6b) and Shannon (Fig. S15a). Meanwhile, we assessed the differences in microbiome composition among different treatment groups using β-diversity. The principal coordinate analysis (PCoA) plots (Fig. 6c) and hierarchical clustering heat map (Fig. S15b) showed overall structure shift of gut microbiota in the DSS induced colitis mice group (DSS) compared with that of the healthy mice. In contrast, the Ce12@CD NPs-treated group and healthy control group clustered closely, the results suggest a relatively close similarity in the microbiota between these two groups. In terms of bacterial composition at the phylum level (Fig. S16a), the DSS-induced colitis mice were obvious with microbial signatures of dysbiosis. A substantial imbalance observed across four major gut bacterial phyla including Firmicutes, Bacteroidetes, Proteobacteria and Actinobacteria, which also is consistent with previous observations in the IBD patients [51].

However, treatment with Ce12@CD NPs was found to effectively reverse the alterations in gut microbiota, leading to a significant increase in the relative abundance of Bacteroidota and a decrease in the relative abundance of detrimental Proteobacteria in DSS-colitis mice (Fig. S16a, S17a and S17b). At the order level (Fig. S16b), which showed that Ce12@CD NPs treatment significantly enhanced the relative abundance of Bacteroidales and Lactobacillus, which are known to confer beneficial effects in animal models of IBD.

The bacterial community composition was further analyzed in detail at the family level (Fig. 6d). During active inflammation, excessive ROS can promote the proliferation of facultative anaerobic bacteria, such as Enterobacteriaceae, leading to dyregulation of the gut microbiota in IBD. Therefore, these abnormally enhanced Escherichia coli strains associated with IBD possess the capability to invade epithelial cells, trigger apoptosis in dendritic cells, and induce the release of proinflammatory cytokines like TNF-α and IL-6 [52,53]. As described, there was a significant increase in the relative abundance of Enterobacteriaceae following DSS induction.

Surprisingly, Ce12@CD NPs treatment was linked to a reduction in the abundance of Enterobacteriaceae, suggesting a possible modulation effect (Fig. 6d and e) and Escherichia coli (Fig. S17c), restoring their levels to those observed in the healthy control group. Furthermore, there was a notable increase in the relative abundance of Muribaculaceae (known for its anti-inflammatory effects) after treatment with Ce12@CD NPs (Fig. 6f). To identify important biomarkers and dominant bacterial communities responsible for the impact on DSS-induced colitis mice within each group, we utilized linear discriminant analysis effect size (LEFSe) analysis (Fig. 6g, Fig. S18). As shown in Fig. 6g, the dysbiosis of gut microbiota in the DSS group was primarily attributed to bacteria belonging to the Bacteroides genus (from the family Bacteroidaceae) and the Lachnospiraceae family (from the order Lachnospirales). The population of Enterobacteriaceae and Escherichia shigella pathogens exhibited a significant increase in colitis mice (LDA (log10) $>$ 3.0), while the aforementioned probiotics, such as Muribaculum and Ruminococcaceae were enriched in Ce12@CD NPs treatment group. These probiotics may influence the gut by potentially inhibiting harmful microbes and affecting mucosal immune homeostasis [45].

Taken together, Ce12@CD NPs treatment significantly enhanced microbial biodiversity and altered the gut microbiota composition. The introduction of Ce12@CD NPs is beneficial in modulating the intestinal flora to treat colitis, which could be attributed to promoting probiotics' growth, and suppressing pathogenic bacteria involved in the onset of IBD.

## 4. Conclusion

In summary, we developed a drug-free Ce12@CD NPs with multiple RONS scavenging activities with an average size of 50 nm for the efficient treatment of IBD. The obtained Ce12@CD NPs possessed SOD, CAT-like enzyme activities and showed effective scavenging ability for multiple RONS including $H_2O_2$, $O_2^{\cdot-}$, ·OH, DPPH and ABTS. Ce12@CD NPs shows good biosafety *in vitro* and effectively reduces the levels of ROS generated by oxidative stress as well as various pro-inflammatory factors, thus protecting cells from ROS attack and maintaining normal cell metabolism. In the prevention/treatment of colitis, Ce12@CD NPs effectively alleviated inflammation, including repairing the intestinal mucosal barrier and restoring the length of the colon, by eliminating elevated RONS and down-regulating the inflammation-associated IL-17 TNF, NF-κB, MAPK, JAK-STAT signaling pathways and ROS related genes expression. 16S rRNA sequencing showed that Ce12@CD NPs could remodel gut microbiota composition by inhibiting detrimental bacterial communities and augmenting beneficial bacterial abundance. Taken together, the designed Ce12@CD NPs incorporated both immune modulation and intestinal microecological adjustment to markedly bolster the therapeutic effect against colitis in mice. What's more, Ce12@CD NPs can be effectively excreted through the kidney, liver and intestinal system, ensuring its safety for IBD treatment. Thus, we developed a promising Ce12@CD NPs for the treatment of IBD.

## CRediT authorship contribution statement

**Dan Yang:** Writing – original draft, Investigation, Data curation. **Rong Wang:** Writing – original draft, Formal analysis. **Lei Zhao:** Software, Methodology. **Ye Xu:** Software, Data curation. **Yufeng Zhu:** Software, Formal analysis. **Jingyan Zhang:** Supervision. **Zhiguo Zhou:** Supervision. **Yun Sun:** Writing – review & editing, Supervision, Investigation. **Shiping Yang:** Project administration. **Hong Yang:** Writing – review & editing, Supervision, Conceptualization. **Wu Wang:** Supervision, Project administration, Funding acquisition.

## Declaration of competing interest

The authors declare that they have no known competing financial interests or personal relationships that could have appeared to influence the work reported in this paper.

## Acknowledgements

This work was supported by the Natural Science Foundation of China (Project No. 22377014); and Construction of Traditional Chinese Medicine Inheritance and Innovation Development Demonstration Pilot Projects in Pudong New Area - High-Level Research-Oriented Traditional Chinese Medicine Hospital Construction (Project No. YC-2023-0901)

## Appendix A. Supplementary data

Supplementary data to this article can be found online at https://doi.org/10.1016/j.mtbio.2025.101705.

## Data availability

Data will be made available on request.

## References

[1] A. Binienda, J. Fichna, M. Salaga, Recent advances in inflammatory bowel disease therapy, Eur. J. Pharmaceut. Sci. 155 (2020), https://doi.org/10.1016/j.ejps.2020.105550.
[2] M.L. Wilson, K.A. Fleming, M.A. Kuti, L.M. Looi, N. Lago, K. Ru, Pathology and laboratory medicine in low-income and middle-income countries 1: access to pathology and laboratory medicine services: a crucial gap, Lancet 391 (10133) (2018) 1927–1938, https://doi.org/10.1016/s0140-6736(18)30458-6.
[3] S.S. Seyedian, F. Nokhostin, M.D. Malamir, A review of the diagnosis, prevention, and treatment methods of inflammatory bowel disease, J. Med. Life. 12 (2) (2019) 113–122, https://doi.org/10.25122/jml-2018-0075.
[4] J. Zhao, W. Gao, X. Cai, J. Xu, D. Zou, Z. Li, B. Hu, Y. Zheng, Nanozyme-mediated catalytic nanotherapy for inflammatory bowel disease, Theranostics 9 (10) (2019) 2843–2855, https://doi.org/10.7150/thno.33727.
[5] G. Jena, P.P. Trivedi, B. Sandala, Oxidative stress in ulcerative colitis: an old concept but a new concern, Free Radic. Res. 46 (11) (2012) 1339–1345, https://doi.org/10.3109/10715762.2012.717692.
[6] A. Piechota-Polanczyk, J. Fichna, Review article: the role of oxidative stress in pathogenesis and treatment of inflammatory bowel diseases, Naunyn-Schmiedebergs Arch Pharmacol 387 (7) (2014) 605–620, https://doi.org/10.1007/s00210-014-0985-1.
[7] Y. Lei, K. Wang, L. Deng, Y. Chen, E.C. Nice, C. Huang, Redox regulation of inflammation: old elements, a new story, Med. Res. Rev. 35 (2) (2015) 306–340, https://doi.org/10.1002/med.21330.
[8] C.C. Winterbourn, Reconciling the chemistry and biology of reactive oxygen species, Nat. Chem. Biol. 4 (5) (2008) 278–286, https://doi.org/10.1038/nchembio.85.
[9] K.M. Poole, C.E. Nelson, R.V. Joshi, J.R. Martin, M.K. Gupta, S.C. Haws, T. E. Kavanaugh, M.C. Skala, C.L. Duvall, ROS-responsive microspheres for on demand antioxidant therapy in a model of diabetic peripheral arterial disease, Biomaterials 41 (2015) 166–175, https://doi.org/10.1016/j.biomaterials.2014.11.016.
[10] S. Massironi, C. Viganò, A. Palermo, L. Pirola, G. Mulinacci, M. Allocca, L. Peyrin-Biroulet, S. Danese, Inflammation and malnutrition in inflammatory bowel disease, Lancet Gastroenterol 8 (6) (2023) 579–590, https://doi.org/10.1016/S2468-1253(23)00011-0.
[11] T. Dassopoulos, S. Sultan, Y.T. Falck-Ytter, J.M. Inadomi, S.B. Hanauer, American Gastroenterological Association Institute technical review on the use of thiopurines, methotrexate, and anti-TNF-α biologic drugs for the induction and maintenance of remission in inflammatory Crohn's disease, Gastroenterology 145 (6) (2013), https://doi.org/10.1053/j.gastro.2013.10.046.
[12] Q. Zhang, H. Tao, Y. Lin, Y. Hu, H. An, D. Zhang, S. Feng, H. Hu, R. Wang, X. Li, J. Zhang, A superoxide dismutase/catalase mimetic nanomedicine for targeted therapy of inflammatory bowel disease, Biomaterials 105 (2016) 206–221, https://doi.org/10.1016/j.biomaterials.2016.08.010.
[13] L.B. Vong, T. Yoshitomi, H. Matsui, Y. Nagasaki, Development of an oral nanotherapeutics using redox nanoparticles for treatment of colitis-associated colon cancer, Biomaterials 55 (2015) 54–63, https://doi.org/10.1016/j.biomaterials.2015.03.037.
[14] N.G. Kotla, S. Rana, G. Sivaraman, O. Sunnapu, P.K. Vemula, A. Pandit, Y. Rochev, Bioresponsive drug delivery systems in intestinal inflammation: state-of-the-art and future perspectives, Adv. Drug Delivery. Rev. 146 (2019) 248–266, https://doi.org/10.1016/j.addr.2018.06.021.
[15] M. Naeem, M.A. Oshi, J. Kim, J. Lee, J. Cao, H. Nurhasni, E. Im, Y. Jung, J.-W. Yoo, pH-triggered surface charge-reversal nanoparticles alleviate experimental murine colitis via selective accumulation in inflamed colon regions, Nanomed. Nanotechnol. Biol. Med. 14 (3) (2018) 823–834, https://doi.org/10.1016/j.nano.2018.01.003.
[16] K.M. Nash, S. Ahmed, Nanomedicine in the ROS-mediated pathophysiology: applications and clinical advances, Nanomed. Nanotechnol. Biol. Med. 11 (8) (2015) 2033–2040, https://doi.org/10.1016/j.nano.2015.07.003.
[17] M. Zeeshan, H. Ali, S. Khan, M. Mukhtar, M.I. Khan, M. Arshad, Glycyrrhizic acid-loaded pH-sensitive poly-(lactic-co-glycolic acid) nanoparticles for the amelioration of inflammatory bowel disease, Nanomed 14 (15) (2019) 1945–1969, https://doi.org/10.2217/nnm-2018-0415.
[18] A. Stallmach, S. Hagel, T. Bruns, Adverse effects of biologics used for treating IBD, Best Pract. Res. Clin. Gastroenterol. 24 (2) (2010) 167–182, https://doi.org/10.1016/j.bpg.2010.01.002.
[19] C.A. Ferreira, D. Ni, Z.T. Rosenkrans, W. Cai, Scavenging of reactive oxygen and nitrogen species with nanomaterials, Nano Res. 11 (10) (2018) 4955–4984, https://doi.org/10.1007/s12274-018-2092-y.
[20] W. Fu, L. Xu, Z. Chen, L. Kan, Y. Ma, H. Qian, W. Wang, Recent advances on emerging nanomaterials for diagnosis and treatment of inflammatory bowel disease, J. Control. Release. 363 (2023) 149–179, https://doi.org/10.1016/j.jconrel.2023.09.033.
[21] C. Liu, L. Gui, J.-J. Zheng, Y.-Q. Xu, B. Song, L. Yi, Y. Jia, A. Taledaohan, Y. Wang, X. Gao, Z.-Y. Qiao, H. Wang, Z. Tang, Intrinsic strain-mediated ultrathin ceria nanoantioxidant, J. Am. Chem. Soc. 145 (34) (2023) 19086–19097, https://doi.org/10.1021/jacs.3c07048.
[22] L. Liu, C. Lu, Z. Tao, Z. Zha, H. Wang, Z. Miao, 2D is better: engineering polydopamine into cationic nanosheets to enhance anti-inflammatory capability, Adv. Healthc. Mater. 13 (18) (2024) 2400048, https://doi.org/10.1002/adhm.202400048.
[23] Q. Huang, Y. Yang, Y. Zhu, Q. Chen, T. Zhao, Z. Xiao, M. Wang, X. Song, Y. Jiang, Y. Yang, J. Zhang, Y. Xiao, Y. Nan, W. Wu, K. Ai, Oral metal-free melanin nanozymes for natural and durable targeted treatment of inflammatory bowel disease (IBD), Small 19 (19) (2023) e2207350, https://doi.org/10.1002/smll.202207350.
[24] C. Shi, J. Dawulieti, F. Shi, C. Yang, Q. Qin, T. Shi, L. Wang, H. Hu, M. Sun, L. Ren, F. Chen, Y. Zhao, F. Liu, M. Li, L. Mu, D. Liu, D. Shao, K.W. Leong, J. She, A nanoparticulate dual scavenger for targeted therapy of inflammatory bowel disease, Sci. Adv. 8 (4) (2022) eabj2372, https://doi.org/10.1126/sciadv.abj2372.
[25] A. Gulbake, A. Jain, A. Jain, A. Jain, S.K. Jain, Insight to drug delivery aspects for colorectal cancer, World J. Gastroenterol. 22 (2) (2016) 582–599, https://doi.org/10.3748/wjg.v22.i2.582.
[26] A. Kumar, S. Das, P. Munusamy, W. Self, D.R. Baer, D.C. Sayle, S. Seal, Behavior of nanoceria in biologically-relevant environments, Environ. Sci. Nano 1 (6) (2014) 516–532, https://doi.org/10.1039/C4EN00052H.
[27] F. Zeng, Y. Shi, C. Wu, J. Liang, Q. Zhong, K. Briley, B. Xu, Y. Huang, M. Long, C. Wang, J. Chen, Y. Tang, X. Li, M. Jiang, L. Wang, Q. Xu, L. Yang, P. Chen, S. Duan, J. Xie, C. Li, Y. Wu, A drug-free nanozyme for mitigating oxidative stress and inflammatory bowel disease, J. Nanobiotechnol. 20 (1) (2022) 107, https://doi.org/10.1186/s12951-022-01319-7.
[28] R. Das, R. Sarma, J.B. Baruah, A hexanuclear cerium(IV) cluster with mixed coordination environment, Inorg. Chem. Commun. 13 (6) (2010) 793–795, https://doi.org/10.1016/j.inoche.2010.03.050.
[29] J. Liu, T. Luo, Y. Xue, L. Mao, P.J. Stang, M. Wang, Hierarchical self-assembly of discrete metal-organic cages into supramolecular nanoparticles for intracellular protein delivery, Angew. Chem. Int. Ed. 60 (10) (2021) 5429–5435, https://doi.org/10.1002/anie.202013904.
[30] J. Liu, J. Sheng, L. Shao, Q. Zheng, W. Li, X. Chen, L. Mao, M. Wang, Tetraphenylethylene-featured fluorescent supramolecular nanoparticles for intracellular trafficking of protein delivery and neuroprotection, Angew. Chem. Int. Ed. 60 (51) (2021) 26740–26746, https://doi.org/10.1002/anie.202111213.
[31] N. Krishna Chandar, R. Jayavel, Wet chemical synthesis and characterization of pure and cerium doped Dy2O3 nanoparticles, J. Phys. Chem. Solids. 73 (9) (2012) 1164–1169, https://doi.org/10.1016/j.jpcs.2012.05.009.
[32] S. Li, L. Zhang, B. Wang, M. Ma, P. Xing, X. Chu, Y. Zhang, A. Hao, An easy approach for constructing vesicles by using aromatic molecules with β-cyclodextrin, Soft Matter 11 (9) (2015) 1767–1777, https://doi.org/10.1039/C4SM02339K.
[33] H. Poudel, A.B. Rangumagar, P. Singh, A. Oluremi, N. Ali, F. Watanabe, J. Batta-Mpouma, J.W. Kim, A. Ghosh, A. Ghosh, Guar-based injectable hydrogel for drug delivery and in vitro bone cell growth, Bioengineering 10 (9) (2023) 1088, https://doi.org/10.3390/bioengineering10091088.
[34] S. Li, L. Zhang, B. Wang, M. Ma, P. Xing, X. Chu, Y. Zhang, A.J.S.M. Hao, An easy approach for constructing vesicles by using aromatic molecules with β-cyclodextrin, Soft Matter 11 (9) (2015) 1767–1777, https://doi.org/10.1039/C4SM02339K.
[35] X. Shan, K. Jiang, J. Li, Y. Song, J. Han, Y. Hu, Preparation of β-cyclodextrin inclusion complex and its application as an intumescent flame retardant for epoxy, Polymers 11 (1) (2019) 71, https://doi.org/10.3390/polym11010071.
[36] F. Zhou, M. Li, M. Chen, M. Chen, X. Chen, Z. Luo, K. Cai, Y. Hu, Redox homeostasis strategy for inflammatory macrophage reprogramming in rheumatoid arthritis based on ceria oxide nanozyme-complexed biopolymeric micelles, ACS Nano 17 (5) (2023) 4358–4372, https://doi.org/10.1021/acsnano.2c09127.
[37] M. Moskvin, I. Marková, H. Malínská, D. Miklánková, M. Hüttl, O. Oliyarnyk, O. Pop-Georgievski, A. Zhigunov, E. Petrovský, D. Horák, Cerium oxide-decorated γ-Fe2O3 nanoparticles: design, synthesis and in vivo effects on parameters of

oxidative stress, Front. Chem. 8 (2020) 682–695, https://doi.org/10.3389/fchem.2020.00682.
[38] P. Ma, R. Wan, Y. Wang, F. Hu, D. Zhang, J. Niu, J. Wang, Coordination-driven self-assembly of a 2D graphite-like framework constructed from high-nuclear Ce10 cluster encapsulated polyoxotungstates, Inorg. Chem. 55 (2) (2016) 918–924, https://doi.org/10.1021/acs.inorgchem.5b02473.
[39] Q. Weng, H. Sun, C. Fang, F. Xia, H. Liao, J. Lee, J. Wang, A. Xie, J. Ren, X. Guo, F. Li, B. Yang, D. Ling, Catalytic activity tunable ceria nanoparticles prevent chemotherapy-induced acute kidney injury without interference with chemotherapeutics, Nat. Commun. 12 (1) (2021) 1436, https://doi.org/10.1038/s41467-021-21714-2.
[40] R. Kopelent, J.A. Van Bokhoven, J. Szlachetko, J. Edebeli, C. Paun, M. Nachtegaal, O.V. Safonova, Catalytically active and spectator Ce3+ in ceria-supported metal catalysts, Angew. Chem. Int. Ed. 54 (30) (2015) 8728–8731, https://doi.org/10.1002/anie.201503022.
[41] Y.G. Kim, Y. Lee, N. Lee, M. Soh, D. Kim, T. Hyeon, Ceria-based therapeutic antioxidants for biomedical applications, Adv. Mater. 36 (10) (2024) 2210819, https://doi.org/10.1002/adma.202210819.
[42] F. Zeng, Y. Shi, C. Wu, J. Liang, Q. Zhong, K. Briley, B. Xu, Y. Huang, M. Long, C. Wang, J. Chen, Y. Tang, X. Li, M. Jiang, L. Wang, Q. Xu, L. Yang, P. Chen, S. Duan, J. Xie, C. Li, Y. Wu, A drug-free nanozyme for mitigating oxidative stress and inflammatory bowel disease, J Nanobiotechnology 20 (1) (2022) 107, https://doi.org/10.1186/s12951-022-01319-7.
[43] J. Pravda, Radical induction theory of ulcerative colitis, World J. Gastroenterol. 11 (16) (2005) 2371–2384, https://doi.org/10.3748/wjg.v11.i16.2371.
[44] R. Li, Y. Fan, L. Liu, H. Ma, D. Gong, Z. Miao, H. Wang, Z. Zha, Ultrathin hafnium disulfide atomic crystals with ROS-scavenging and colon-targeting capabilities for inflammatory bowel disease treatment, ACS Nano 16 (9) (2022) 15026–15041, https://doi.org/10.1021/acsnano.2c06151.
[45] T. Jin, H. Lu, Q. Zhou, D. Chen, Y. Zeng, J. Shi, Y. Zhang, X. Wang, X. Shen, X. Cai, H2S-Releasing versatile montmorillonite nanoformulation trilogically renovates the gut microenvironment for inflammatory bowel disease modulation, Adv. Sci. 11 (14) (2024) 2308092, https://doi.org/10.1002/advs.202308092.
[46] L. Wang, Y. Hu, B. Song, Y. Xiong, J. Wang, D. Chen, Targeting JAK/STAT signaling pathways in treatment of inflammatory bowel disease, Inflamm. Res. 70 (7) (2021) 753–764, https://doi.org/10.1007/s00011-021-01482-x.
[47] F. Scaldaferri, M. Sans, S. Vetrano, C. Correale, V. Arena, N. Pagano, G. Rando, F. Romeo, A.E. Potenza, A. Repici, A. Malesci, S. Danese, The role of MAPK in governing lymphocyte adhesion to and migration across the microvasculature in inflammatory bowel disease, Eur. J. Immunol. 39 (1) (2009) 290–300, https://doi.org/10.1002/eji.200838316.
[48] T. Zhang, J. Jiang, J. Liu, L. Xu, S. Duan, L. Sun, W. Zhao, F. Qian, MK2 is required for neutrophil-derived ROS production and inflammatory bowel disease, Front. Med. 7 (2020), https://doi.org/10.3389/fmed.2020.00207.
[49] C. Zhang, H. Wang, X.H. Yang, Z. Fu, X.R. Ji, Y.F. Shi, J. Zhong, W.G. Hu, Y.Q. Ye, Z.T. Wang, D.L. Ni, Oral zero-valent-molybdenum nanodots for inflammatory bowel disease therapy, Sci. Adv. 8 (37) (2022), https://doi.org/10.1126/sciadv.abp9882.
[50] R. Caruso, B.C. Lo, G.J.N.R.I. Núñez, Host–microbiota interactions in inflammatory bowel disease, Nat. Rev. Immunol. 20 (7) (2020) 411–426, https://doi.org/10.1038/s41577-019-0268-7.
[51] M.T. Alam, G.C.A. Amos, A.R.J. Murphy, S. Murch, E.M.H. Wellington, R. P. Arasaradnam, Microbial imbalance in inflammatory bowel disease patients at different taxonomic levels, Gut Pathog. 12 (2020) 1, https://doi.org/10.1186/s13099-019-0341-6.
[52] S.E. Winter, M.G. Winter, M.N. Xavier, P. Thiennimitr, V. Poon, A.M. Keestra, R. C. Laughlin, G. Gomez, J. Wu, S.D. Lawhon, Host-derived nitrate boosts growth of E. coli in the inflamed gut, Science 339 (6120) (2013) 708–711, https://doi.org/10.1126/science.1232467.
[53] Z. Shi, X. Li, J. Chen, Z. Dai, Y. Zhu, T. Wu, Q. Liu, H. Qin, Y. Zhang, H. Chen, Enzyme-like biomimetic oral-agent enabling modulating gut microbiota and restoring redox homeostasis to treat inflammatory bowel disease, Bioact. Mater. 35 (2024) 167–180, https://doi.org/10.1016/j.bioactmat.2024.01.016.